EARTH SCIENCES

Using a portable XRF spectrometer to determine geochemical and spatial correlations between alteration and gold mineralization in the Beaver Dam deposit, Nova Scotia

Jessica Guselle

Submitted in partial fulfillment of the requirements for the degree of Bachelor of Science, Honours

Department of Earth Science, Dalhousie University, Halifax, NS

March 2012

Distribution License

DalSpace requires agreement to this non-exclusive distribution license before your item can appear on DalSpace.

NON-EXCLUSIVE DISTRIBUTION LICENSE

You (the author(s) or copyright owner) grant to Dalhousie University the non-exclusive right to reproduce and distribute your submission worldwide in any medium.

You agree that Dalhousie University may, without changing the content, reformat the submission for the purpose of preservation.

You also agree that Dalhousie University may keep more than one copy of this submission for purposes of security, back-up and preservation.

You agree that the submission is your original work, and that you have the right to grant the rights contained in this license. You also agree that your submission does not, to the best of your knowledge, infringe upon anyone's copyright.

If the submission contains material for which you do not hold copyright, you agree that you have obtained the unrestricted permission of the copyright owner to grant Dalhousie University the rights required by this license, and that such third-party owned material is clearly identified and acknowledged within the text or content of the submission.

If the submission is based upon work that has been sponsored or supported by an agency or organization other than Dalhousie University, you assert that you have fulfilled any right of review or other obligations required by such contract or agreement.

Dalhousie University will clearly identify your name(s) as the author(s) or owner(s) of the submission, and will not make any alteration to the content of the files that you have submitted.

If you have questions regarding this license please contact the repository manager at dalspace@dal.ca.

Grant the distribution license by signing and dating below.

_____ _____

Name of signatory Date

DALHOUSIE UNIVERSITY
Inspiring Minds

Department of Earth Sciences
Halifax, Nova Scotia
Canada B3H 4J1
(902) 494-2358
FAX (902) 494-6889

DATE: April 30/12

AUTHOR: Jessica Guselle

TITLE: Using a portable XRF spectrometer to determine geochemical and spatial correlations between alteration and gold mineralization in the Beaver Dam deposit, NS

Degree: BSc Convocation: May Year: 2012

Abstract

The Beaver Dam deposit is a metaturbidite-hosted mesothermal gold deposit, consisting primarily of slate with subordinate metagrewacke, and bedding-parallel auriferous quartz veins which contain variable amounts of carbonate. The purpose of this study is to use a whole rock lithogeochemistry approach on a large number of samples to determine whether there are geochemical and spatial correlations between hydrothermal alteration and gold mineralization. A portable X-ray fluorescence (XRF) spectrometer was used to analyze over 5000 samples. Each sample consists of pulps of drill core sampled at one meter intervals irrespective of lithology, quartz veins, or alteration. These samples were collected from over 50 drill holes within and surrounding the mineralized zone of the property with an overall strike length approximately 140m and 50m across strike. A set of 10 samples was reanalyzed 10 times each to ensure the reproducibility of the data. A subset of 30 samples was analyzed by ICP-MS to test the accuracy of the XRF spectrometer. The ICP-MS data were plotted against the XRF data to visually assess the accuracy of the XRF data. Most elemental plots created linear trends with a slope close to or equal to one.

The coarser clastic metasedimentary rocks are dominated by silica which dilutes other major and trace element concentrations, but are enriched in denser detrital minerals such as zircon. In contrast, the finer grained rocks are relatively depleted in silica and enriched in elements reflecting higher concentrations of micas and clays (eg. K, Rb, Ba) and the redox sensitive transition elements (Ti, V, Cr). Bivariate plots of V vs. Ti, V vs. Cr, and Ti vs. Cr show very good correlation (R^2=0.85). These plots characterize the broad lithological groups, including quartz veins with concentrations approaching the origin, sandstones having lower relative concentrations of these elements, and slates having higher concentrations of these elements. The very good correlation of these elements and distribution of concentrations likely reflect the general immobility of Ti, V, and Cr during hydrothermal alteration. When plotted against Ti and V, samples with elevated Mn and Ca concentrations likely reflect carbonate associated with quartz veins or naturally occurring in the host rock. Plots of K, Rb, Ba, and Sr vs. Ti and V show good correlation indicating that there is little to no mobility of alkali and alkaline elements. Of other elements plotted against the immobile elements, a small proportion of samples show slight elevations in As and Zn concentrations, suggesting these were introduced during alteration. However, when plotted against Au, As and Zn show a very weak correlation, and therefore may not have been introduced into the deposit at the same time as the gold. The nature of the sampling protocol of this study (which was taken at 1 m intervals down each drill core, conducted irrespective of lithology, quartz veining, or alteration) may have had an effect on the reliability of this data, and is responsible for the apparent mixing zone between lithological groups. The average of the fine fraction of gold from two analyses by fire assay was used to avoid the nugget effect having an effect in our results. The gold may have been introduced late or remobilized during late stage quartz veining. A plot of Au vs. V does show however, that the fine fraction gold is preferentially concentrated in the slates. To determine the spatial distribution, this information was generated into spatial sections, which confirm a very weak to non-correlation between alteration and gold on a scale greater than the 1 m sampling intervals.

Table of Contents

List of Figures

Acknowledgements

I would like to thank the faculty and staff in Dalhousie University's Earth Science department for their incredible instruction and support during my undergraduate degree. Also, thank you to my friends, peers and the Dawson Club, who have all been a great support system over the course of this thesis. I would also like to thank Acadian Mining for providing the drill core, XRF spectrometer, and invaluable expertise and support for my project. In particular, my co-supervisor Rick Horne, as well as Drew Pelley, Adam Sherry, Tom Melanson, and Mike Walsh for their great advice and assistance with my large amount of data. I would also like to thank Richard Cox and Dan Kontak for all of their helpful geochemical advice. Finally, I would like to thank my supervisor Mike Young for his guidance and expertise, both of which have made this experience an enjoyable one.

1.0 Introduction

1.1 Introduction to the problem

Turbidite-hosted hydrothermal veins are a main depositional source of gold, which may be structurally or stratigraphically controlled, and most classically concentrate in vertically stacked saddle reefs in anticlinal fold hinges (Robert *et al.*, 2007). Only three turbidite-hosted gold districts worldwide contain over 10Moz Au, however this deposit style has hosted over 140 Moz Au globally (Robert *et al.*, 2007). Turbidite sequences occur as graded sedimentary sequences as a result of marine gravity flows ranging in age from the Archean to Tertiary in age (Bierlein *et al.*, 1998). These sequences typically consist of metamorphosed greywackes, siliceous wackes, shales, and carbonaceous shales with a metamorphic grade ranging from greenschist to amphibolite facies (McMillan, 1996). Lode gold deposits characteristically are found within stratabound quartz veins that range in size, and can be either bedding-parallel or discordant (McMillan, 1996). These quartz veins often concentrate within the hinges of anticlinal folds (called saddle reef deposits), with gold being concentrated in the bedding-parallel veins that often exhibit a laminated texture (Kontak and Smith, 1993). This laminated texture which is being described is also often referred to as a "crack-seal" or "ribbon" texture, representing dynamic quartz veins which have been episodically reopened with additional quartz precipitation due to oscillations in the fluid pressure. Gold can also concentrate in the discordant quartz veins and as segregations, as well as being disseminated within the sedimentary host rock or filling late brittle faults and fractures (Bierlein *et al.*, 1998). Often the mineralogical paragenesis of these veins are relatively simple, and consists predominately of quartz, with minor

amounts of carbonate, native gold, and sulphide minerals, with arsenopyrite being the most abundant sulphide (Kontak and Smith, 1993).

There is a worldwide distribution of these deposits, including Yellowknife (Northwest Territories, Canada), the Otago Goldfield (New Zealand), Salsigne (France), the Cariboo District (British Columbia, Canada), Muruntau (Uzbekistan), the Victorian Goldfields (Southeastern Australia), and the Meguma Terrane (Nova Scotia, Canada) (Beirlein *et al.*, 1998). Analogous slate-hosted gold deposits can be found in the Victorian Goldfields of Australia. The Victorian Goldfields are found within a sequence of thick, metamorphosed turbidite sequences deposited in the Cambro-Devonian (Wilde *et al.*, 2004). The regional geology of the area is generally controlled by the Lachlan Fold Belt system, characterized by north-south trending folds and thrusts and associated greenschist facies metamorphism (Bierlein *et al.*, 1998). Like the Meguma deposits, gold within the Victorian Goldfields are hosted in bedding-parallel quartz veins and auriferous reefs, with their emplacement due to mesothermal activity (Kontak and Smith, 1993).

Wallrock hydrothermal alteration within turbidite-hosted gold deposits is minor, and if it is present at all, it is typically vein-controlled, with the veins having well defined sharp contacts with the enclosing slate, argillite, or greywacke host rock (Bierlein *et al.*, 1998). Typical hydrothermal alteration within the Meguma Terrane is often limited to silica flooding, creating thick bleached zones (Fig.1) and have a wide range (but are minor) in size. Quartz veining is also commonly associated with hydrothermal alteration, with bedding concordant veins varying in thickness from 0.5 cm to 1m (although some veins of 2-3 m thickness may occur) and discordant veins varying in thickness from 1-2 m (Kontak and Smith, 1993).

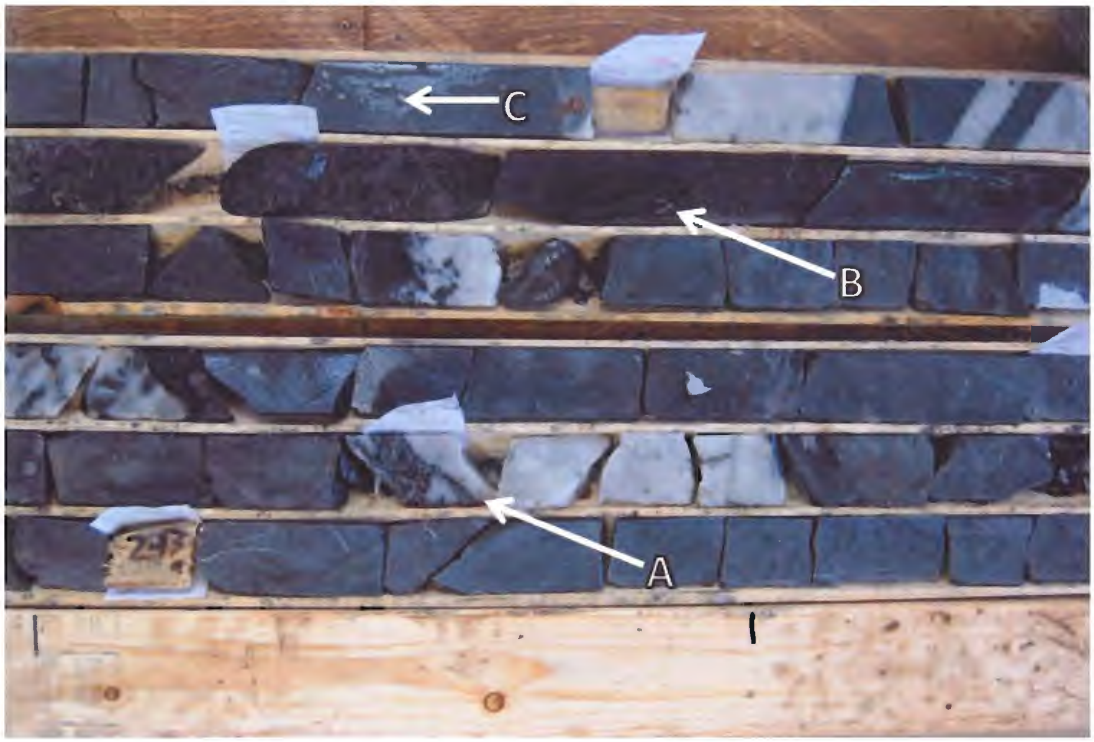

Figure 1. Beaver Dam core box showing (A) concordant veins (some concordant veins have laminated texture which have variable digestion of the wall-rock material), as well as (B) disseminated arsenopyrite, and (C) silica bleaching.

Multiple hypotheses have been proposed to help explain the absence of significant hydrothermal alteration present in these deposits, including that veins formed by magmatic hydrothermal fluids introduced during syngenetic deformation and mineralization, or more current theories which adapt lateral secretion theories which suggest that the quartz veins laminated texture is due to episodic re-opening of veins during formation (McMillan, 1996). However, because these hydrothermal alteration haloes are so difficult to distinguish in outcrop, geochemical analysis has become essential in understanding the alteration which is associated with the metaturbidite-hosted lode gold deposits (Bierlein *et al*, 1998; Pendergast,1997).

1.1.2 Nuggety Gold

Gold-bearing quartz veins are often mined based on visible coarse gold anomalies, which come from the gold's 'nuggety' properties. The "nugget effect" of gold is a term which describes the degree of randomness of gold distribution within a body of mineralization (Dominy *et al.*, 2002). This physical quality of gold causes it to group in 'nuggets' which can therefore skew sampling programs by its distribution (Dominy *et al.,* 2002). A high nugget effect results in severe sampling issues due to the presence of lack of coarse gold in the sample. In addition, the common practice of sub-sampling in standard fire assay procedures leads to similar issues due to the presence of lack of coarse gold in the subsample. To reduce this problem, gold fire assays can be conducted where the coarse fraction of gold (or gold 'nuggets') are physically separated by sieving from the fine fraction of the gold. This procedure is referred to as "screen metallic fire assay", where the sample pulp is passed through a 106 micron mesh. The portion which doesn't pass through (the coarse fraction) is retained and reanalyzed by fire assay to obtain the concentration of Au in the coarse fraction. The fine fraction is the portion of the sample which passes through the 106 micron mesh, and two samples are analyzed by fire assay, with concentration of Au in the fine fraction being reported as the average of these two subanalyzes. The "nugget effect" makes resource estimation difficult as it is difficult to define gold grade zones with confidence.

The purpose of this study is to compare the geochemical and spatial distribution of hydrothermal alteration gold mineralization in order to determine whether there is a commensurate increase in elements thought to be introduced during hydrothermal alteration with increasing gold grades within the Beaver Dam deposit of the Meguma Terrane in Nova Scotia, Canada. Comparison of the duplicate fire assay results for the two fine fraction samples in the

screen fire assay process indicate good reproducibility, suggesting that the fine fraction gold values are representative of the sample. Although duplicate results for the coarse fraction do not exist, it is expected that the coarse character of the gold would result in poor reproducibility. Therefore the results of the whole rock chemistry determined here were compared with the "fine fraction gold" grades.

Prendergast (2007) conducted a whole-rock lithogeochemical study in the St Ives goldfield, Western Australia, in which ICP-MS/OES data were used to determine if there were any pathfinder elements associated with alteration, as well as correlating these data into lithological and stratigraphic domains. The study was successful in using this bulk lithogeochemical approach to effectively identify lithological packages, as well as identifying pathfinder elements As, Bi, Sb, W, and Mo that reflected alteration within the deposit. This approach allowed for a stronger interpretation of the stratigraphic domains as well as reducing the exploration target areas for a more cost-effective drilling program (Prendergast, 2007). In this study, a portable energy dispersive XRF analysis was used as opposed to ICP-MS/OES analysis because it is generally more cost effective and more efficient where the goal was to collect a large number of analyses in minimal time and with minimal cost. In order to determine deposit-scale correlations between hydrothermal alteration reflected in whole rock geochemistry and gold mineralization, a large number of samples are required. The goal of this study is to determine lithological signatures using bivariate plots of trace elements, as well as utilizing pathfinder elements to determine samples which are enriched above the background lithological concentrations. This enrichment is may reflect hydrothermal alteration, and potentially related to the introduction of gold into the deposit.

1.2 Regional Geology and Geologic Setting

1.2.1 The Meguma Group

The Meguma Terrane is located in southern Nova Scotia and is a terrane of the Appalachians. The Meguma Terrane is separated from the Avalon Terrane by the Cobequid-Chedabucto Fault System (Fig. 2). The Meguma Supergroup dominates the Meguma Terrane and is a thick sequence of deep-water metasediments, Cambro-Ordovician in age, and was deformed during the Devonian Acadian Orogeny into open, upright folds trending NE-SW under greenschist to upper amphibolite facies regional metamorphism (Kontak and Smith, 1993).

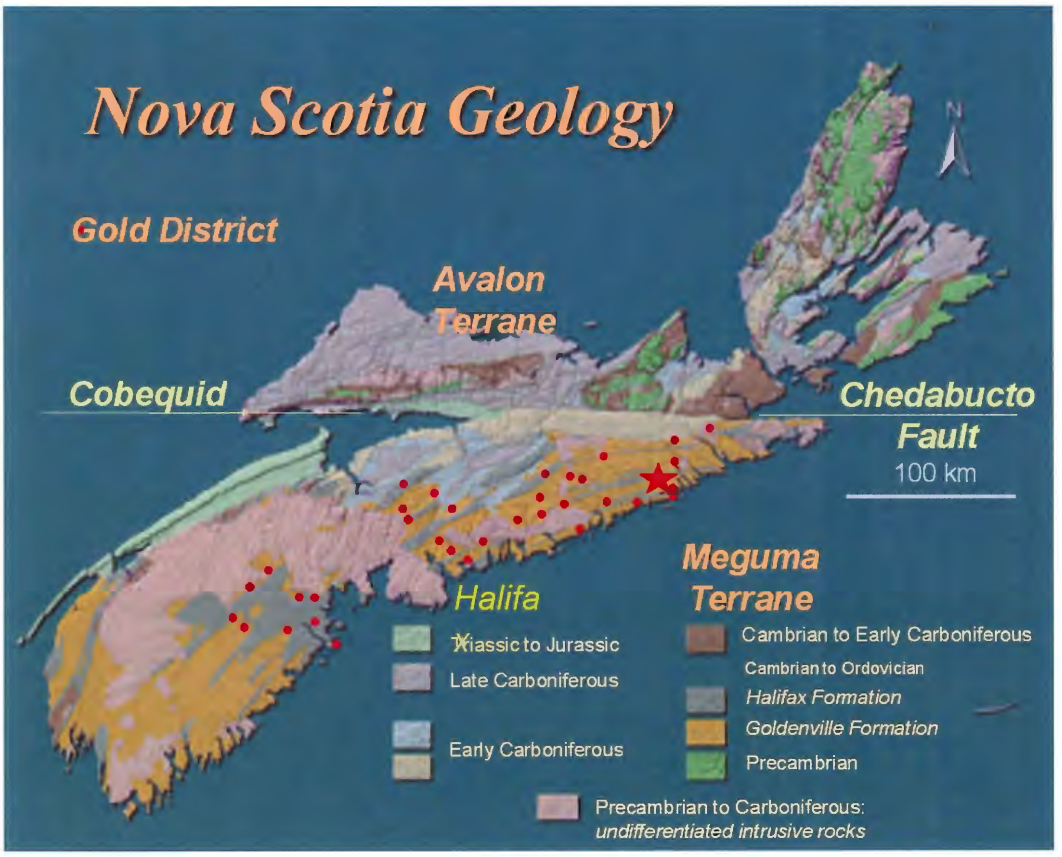

Figure 2.Regional geological map of Nova Scotia with gold districts highlighted.

The Meguma Supergroup is a thick succession of deep-sea to near-shelf fan complexes, and can be further subdivided into distinct formations, the Goldenville Group and the Halifax Group (Schenk, 1997). Recent studies have modified the stratigraphic nomenclature (elevating the Meguma Group to the Meguma Supergroup) (Schenk, 1997).

The Goldenville Group is principally comprised of greenish gray metaquartzarenite, quartzite, metagraywacke, metasiltstone, and slate (Schenk, 1997) with metasandstone-dominated cycles that are interbedded with minor metasiltstone and slate that fine upwards (Horne and Pelley, 2006). These cycles also locally have a fine-grained conglomerate present at the base, as well as sand volcanoes (Horne and Pelley, 2006). Within the hinge area of the Moose River- Beaver Dam- Fifteen Mile Stream Anticline (Fig. 3), it is common to observe disseminated sulphide minerals as well as carbonate alternation visible due to brown spots and weathering (Horne and Pelley, 2006). The stratigraphy of the Goldenville Group has been subdivided into three formations (from youngest to oldest): The Taylor Head Formation, the Tangier Formation, and the Moose River Formation (Horne and Pelley, 2006). The Beaver Dam deposit is situated in the Moose River Formation which is characterized by thick mudstone (metamorphosed to slate) intervals, interbedded with minor metasiltstone. Disseminated sulphides and minor carbonate alteration is common (Horne and Pelley, 2006). This formation hosts the Touquoy zone of the Moose River Gold District, a large zone of low-grade gold mineralization (Horne and Pelley, 2006).

The Halifax Group conformably overlies the Goldenville Group, and is primarily composed of grayish green to black slate and metasiltstone (Horne and Pelley, 2006). The slate and metasiltstone is often finely laminated (cm scale), and some of the black slate is interbedded

with metasiltstone and metasandstone. Sulphide minerals (primarily pyrite and pyrrhotite) are abundant within the Halifax Group (Horne and Pelley, 2006).

1.2.2 Meguma Gold

Gold found within the Meguma Group is primarily concentrated within quartz veins associated with the deformation during the Acadian Orogeny. (Kontak and Smith, 1990). Many

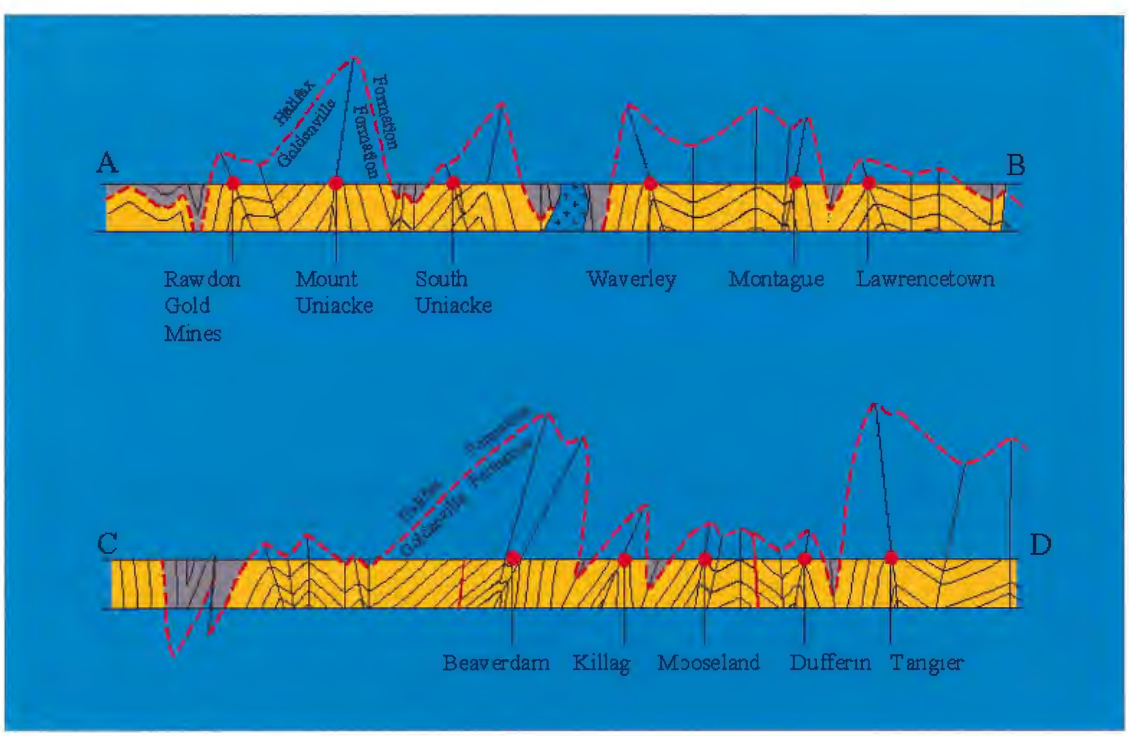

Figure 3. Schematic cross-section of the open, upright folds of the Meguma Supergroup, and the presence of local gold districts (including the Beaver Dam deposit)

gold deposits found in the area are located in anticlinal hinges of these upright folds, including the Beaver Dam deposit itself, which consists of bedding parallel laminated quartz veins cut by discordant veins (Fig. 3).

Gold production from the Meguma gold region has come from over 60 deposits, with grades ranging from 8-50 g/t, and a total of 35.13 tonnes produced from the district (McMillan, 1996). Other turbidite-hosted lode gold deposits, such as the Bendigo field of Australia has had a higher amount of production, with grades ranging from 3-30 g/t and a total over 373 tonnes of non-alluvial gold from over 40Mt of ore since 1851 (McMillan, 1996).

Quartz veins are associated with anticlinal hinges, often taking form as bedding concordant, saddle reef, and discordant veins (Horne and Culshaw, 2001). Based on $^{40}Ar/^{39}Ar$ dating of hydrothermal amphibole, biotite, and muscovite, the veins are estimated to have formed approximately 374 Ma (Kontak and Smith, 1993). The bedding concordant veins vary in thickness from approximately 0.5 cm to 1 m, exhibit a laminated texture, and exhibit a variable degree of deformation (Kontak and Smith, 1993). The discordant veins vary in thickness and can range up to 2-3 m thick, locally also exhibit a laminated texture, and have mutual cross-cutting relations with bedding concordant veins (and are therefore synchronous with bedding concordant veins) (Horne and Culshaw, 2001). They often record more shortening than the bedding concordant veins as they are at high angle to the shortening direction (Kontak and Smith, 1993).

Gold found in the turbidite-hosted deposits is commonly concentrated within the bedding parallel quartz veins, and within the Meguma gold districts, these auriferous quartz veins are typically bedding-parallel, and concentrated in the slate-dominated packages (Ryan and Smith, 1998; Kontak and Smith, 1993; Sangster and Smith, 2007).

1.2.3 The Beaver Dam Deposit

The Beaver Dam deposit is an advanced exploration property, 100% owned by Acadian Mining Corporation, and is their principal project being considered for open pit mining (Fig. 4). The deposit is composed of thickly bedded metasandstone, interbedded with anomalously thick beds of slate (Kontak and Smith, 1990). The gold bearing quartz veins are typically associated with these slate-dominated packages. In more detail, those slate units can be further divided into three distinct packages; the Crouse, Papke, and Austen zones, and the entire deposit is cut by the Mud Lake Fault (Fig. 5) (Kontak and Smith, 1990). Gold in this deposit commonly occurs in bedding concordant and discordant sulfide-bearing quartz veins that exhibit a typical laminated texture, as well as minor amounts of carbonate (Kontak and Smith, 1993).

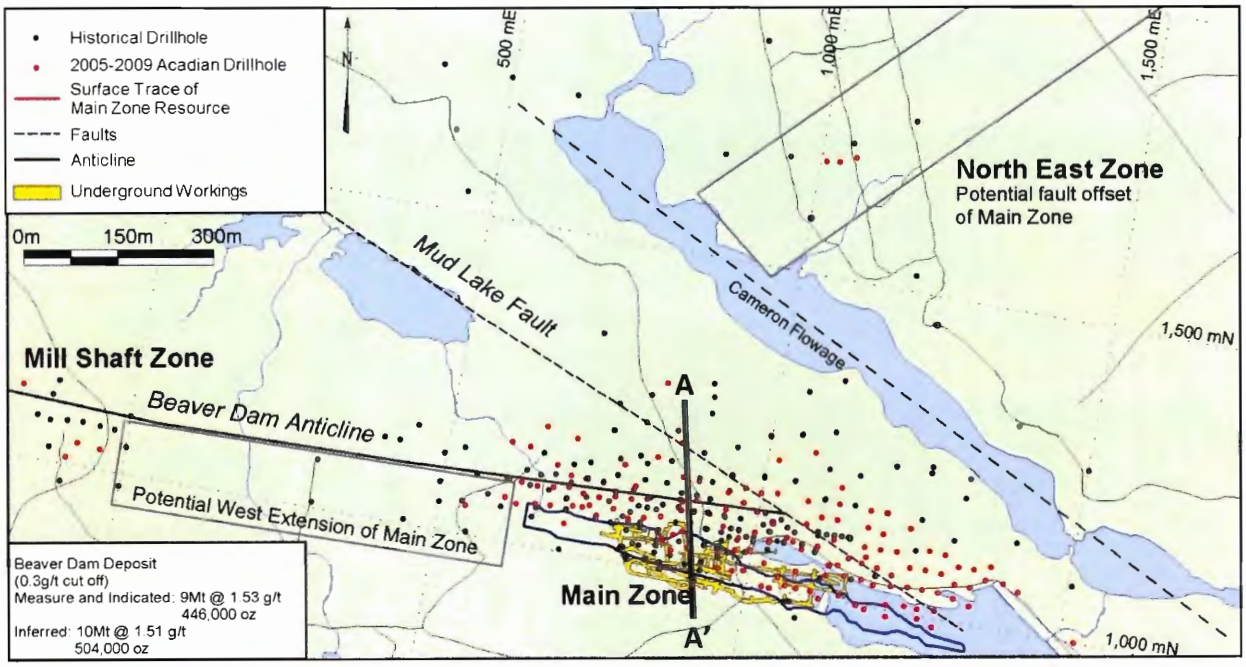

Figure 4. Beaver Dam property map

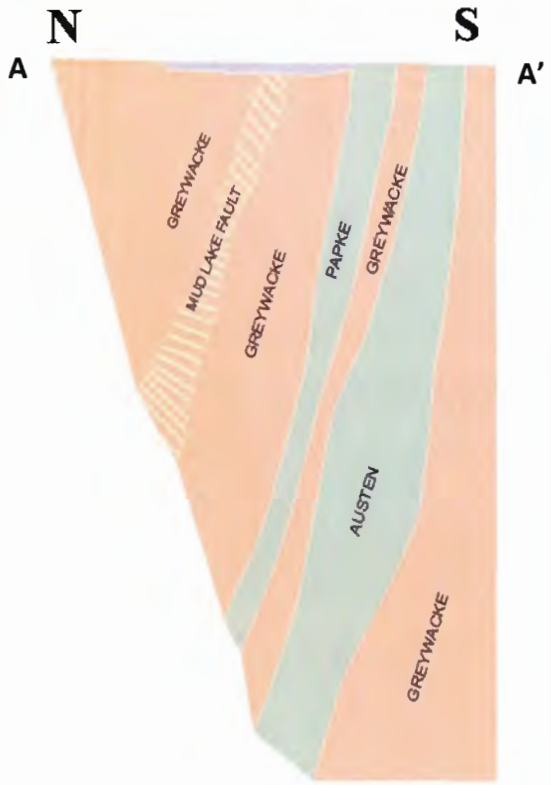

Figure 5. Cross-section of the Beaver Dam deposit (not to scale) showing the main stratigraphic units. (Looking east)

Veins in the Beaver Dam deposit are predominately quartz-rich, however there is great variation in their size, geometry and mineralogy (Kontak and Smith, 1993). Kontak and Smith (1993) characterized vein textures into four types: 1) quartz-rich veins with small amounts of sulphides and/or laminated carbonate present, 2) quartz veins with the laminated or 'crack-seal' texture (which will often incorporate wall-rock material into the veins), 3) coarse-grained 'pegmatoidal' quartz veins, as well as 4) massive bull quartz which may have euhedreal vugs of quartz, calcite, chlorite, albite, muscovite or pyrite. The laminated texture that is described is thought to have formed due to sequential reopening and closing of the quartz veins due to hydrofracturing and mineral precipitation, and there are wall rock inclusions and slivers which impart the laminated texture (Ramsay, 1980).

The mineralogy and vein paragenesis of the Meguma Supergroup (and more specifically within the Beaver Dam deposit) has been summarized by Kontak and Smith (1993) to have two hypogene stages, or stages which have formed by ascending solutions (Figs. 6 and 7). The Stage I mineralogy is dominated by quartz, plagioclase, biotite, and tourmaline, with accessory ilmenite, sulfides, apatite, garnet, hornblende and epidote. Stage II mineralogy (which also occurs as alteration products of stage I minerals, most commonly in bedding-concordant veins) is dominated by Ca-rich plagioclase being replaced by albite, calcite, muscovite, and/or chlorite, biotite being chloritized, ilmenite being replaced by anatase or titanite, and a primary assemblage of chlorite, calcite, pyrite, albite and muscovite which occurs only within the younger discordant veins (Kontak and Smith, 1993). Sulphides present (from most to least abundant) include: arsenopyrite, pyrrhotite, pyrite, chalcopyrite, galena, sphalerite, marcasite, and lollingite with rare molybdenite and Bi-Te sulphides (Fig. 7; Kontak and Smith, 1993). These sulphides occur

as films that coat the vein-wallrock contacts and are proposed to have been introduced late in the paragenetic sequence. Carbonate alteration occurs in the form of clots in both bedding concordant and discordant veins, as well as freely within the wallrock material (Kontak and Smith, 1993).

Kontak and Smith (1993) used amphibole-plagioclase geothermometry to determine the temperature of vein formation in the Beaver Dam deposit. They determined that due to the presence of strongly zoned Ca-rich plagioclase that underwent subsequent albitization, the initial average temperature for Stage I mineralization exceeded 525°C, and the average for Stage II mineralization (which included more Na-rich plagioclase growth) occurring below 375°C (Kontak and Smith, 1993). While these are the averages, it is important to note that there were isolated analyses which yielded temperatures as low as 455°C and 300°C, respectively, by application of oxygen isotope geothermometry to plagioclase-amphibole and quartz-chlorite pairs (Kontak and Smith, 1993). Studies using different geothermometers obtained similar results which were compared in Kontak and Smith (1993), and are summarized in Figure 6.

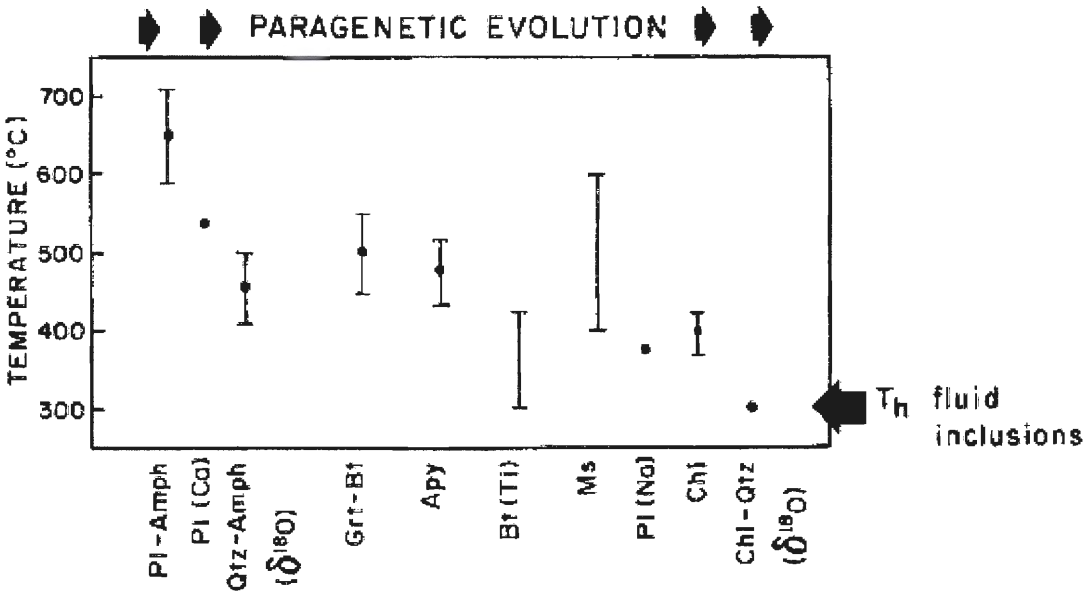

Figure 6. Summary diagram of inferred temperatures of formation of mineral assemblages in the Beaver Dam deposit, as taken from Kontak and Smith, 1993.

Gold found within the Beaver Dam deposit occurs as isolated grains found in the bedding-concordant veins, commonly in proximity to wall-rock contacts, as well as disseminated gold found in the wall-rock adjacent to the veins. Gold found in close proximity to wall-rock contacts is commonly associated with chlorite, calcite, and muscovite alteration (Kontak and Smith, 1993). Gold in the deposit is also found associated as fine-grained disseminations, fracture-controlled veinlets and along grain boundaries within pyrrhotite and aresenopyrite, as well as having grain contacts with galena and chalcopyrite, along fractures cutting altered plagioclase or chloritized biotite, as well as in the wallrock (Kontak and Smith, 1993). Kontak and Smith (1993) proposed that the gold was introduced at the same time as the stage II vein mineralization due to the association with other stage II mineral phases. However, it is also possible that remobilization of earlier gold has also occurred after the Stage II fluid flow (Kontak and Smith, 1993). Kontak and Smith (1993) have used geothermometers to determine the relative hypogene stages which make up the mineral paragenesis, however the timing and

introduction of gold into the system is still poorly understood. They observed auriferous quartz veins cutting arsenopyrite-bearing veins, indicating that the gold could have been potentially remobilized at a lower temperature, post-sulphide mineralization, or potentially being initially introduced at this time. There have been examples of gold occurring in association with arsenopyrite, however there has been no subsequent analyses to determine if gold also occurs within the chemical structure of arsenopyrite.

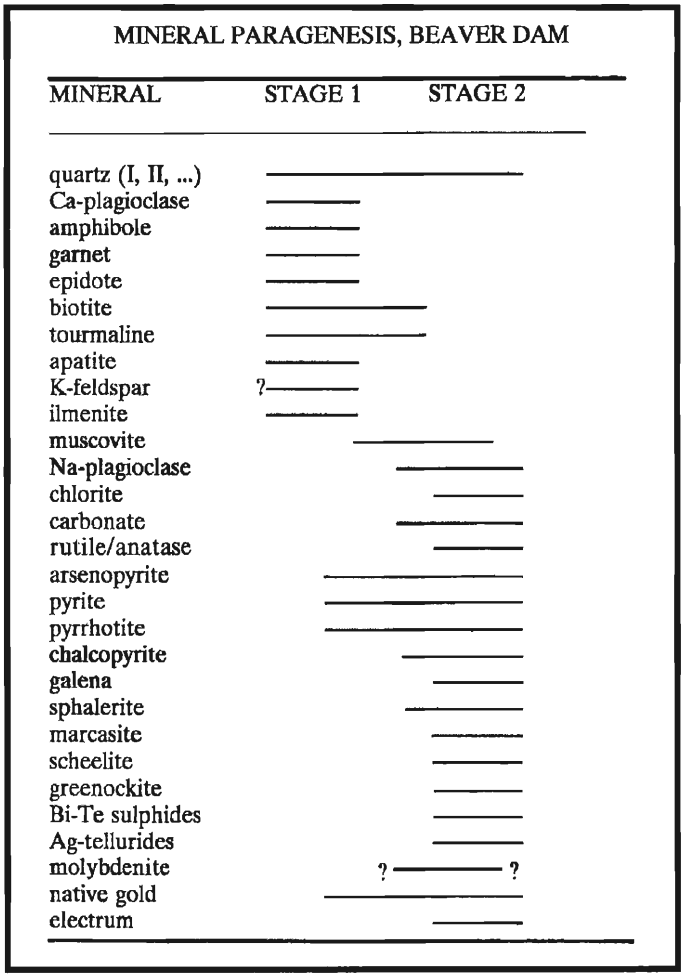

Figure 7. Mineral paragenesis of the Beaver Dam deposit, as taken from Kontak and Smith, 1993.

1.3 *Scope of the Study*

The purpose of this study is to use a whole rock lithogeochemistry approach to ultimately determine the geochemical and spatial distribution of hydrothermal alteration associated with gold in the Beaver Dam Deposit. Before geochemical analysis and interpretation is done, a large portion of this study includes the quality control on XRF analysis to ensure that the data is good. Over 5000 analyses were completed using a portable energy dispersive XRF analysis to establish geochemical trends that can be explained by variations in lithology. The geochemistry which was not explained by lithology is presumably related to veins and related alteration, which was then compared to gold grades both geochemically and spatially.

The sampling protocol for this study is not ideal, and therefore one of the primary focuses of this study is to assess sampling method as well as using an XRF spectrometer as the means of analysis, and once that has been determined, correlations may then be interpreted.

2.0 Methods

2.1 Sample Preparation

The primary method of analysis for this thesis is X-ray fluorescence spectrometry. Drill programs at the Beaver Dam deposit have been taking place since the 1980s, with 153 diamond drill holes being drilled since 2005. Drill core was sampled at 1m intervals irrespective of lithology, alteration, and quartz veining. The sampling was completed during the drilling program. Unfortunately, this sampling protocol has resulted in the mixing of lithological types and quartz veining. Although this sampling protocol will yield mixing zones between the major lithological groups in the geochemical analysis, using such a large sample size will hopefully make the geochemistry of unaltered host rocks and altered zones visible. Regardless of the lithologic mixing within samples, it is thought that the large number of samples analyzed and the scale of the lithologic units in the deposit will allow for any major geochemical variations due to alteration to be reflected in the data.

The drill core was split, with half of its contents being pulverized and powdered. The powdered samples were then subsequently fire assayed for gold. The fire assay analysis was done by ALS Chemex, where a full screen metallics on all samples was completed. Samples were crushed to 106 microns, and the coarse fraction of gold was separated from the remaining fine fraction. Representative material from the coarse and fine fractions were subsequently fire assayed and the weight average was taken from all three. There are three types of samples due to

the analysis of the coarse fraction as well as two analyses of the fine fraction. Two analyses of the fine fraction were taken in order to determine the reproducibility and therefore evaluate the nugget effect on this size fraction. Both of the fine fraction analyses yield very similar results, indicating that the fine fraction is not significantly affected by nuggety gold; the fine fraction is considered to be homogeneous. It is a subsample of the fine fraction that was analyzed in this study.

Samples for XRF analysis were chosen from a subset of drill holes located in the main area of mineralization (Fig. 4). Plastic pill bottles were filled with approximately 3g of powder and covered with cellophane wrap. The powdered samples are homogenous and therefore representative of the sampled core. The samples were then placed on an XRF spectrometer with the cellophane wrapped top facing the x-ray beam for analysis. Pill bottles were cleaned with warm water and soap after use and subsequently reused for analysis.

2.2 X-Ray Fluorescence (XRF)

X-ray fluorescence (XRF) spectrometry was used as the primary method of analysis because it is a non-destructive technique that is more cost and time effective than alternative methods, such as ICP-MS analysis (although it yields at a slightly lower resolution). It can detect whole rock major and trace element chemistry for up to 80 elements as low as parts per million (Rollinson, 1993).

X-rays are high energy photons that carry no mass or charge, and are able to travel great distances (Murphy, 2010). They can be produced in two ways: the acceleration of an electron will yield Bremsstrahlung x-rays, and the transition of energy between electron shells yields

characteristic x-rays (Murphy, 2010). Characteristic x-rays are emitted when electrons or Bremsstrahlung x-rays hit electrons at high speeds and eject them from an atom's inner shell. Electrons from outer shells subsequently drop down to fill these vacancies, thereby emitting a 'characteristic x-ray wavelength' (Murphy, 2010). Characteristic x-rays are important for XRF analysis, as each element has different spaces between electron orbital shells, and therefore there is a precise and measurable amount of energy that is emitted during this process (Murphy, 2010).

Within the XRF spectrometer, a primary x-ray beam excites atoms within the sample with x-rays. This procedure emits many electrons, Bremsstrahlung x-rays, and characteristic x-rays (Rollinson, 1993). Electrons that are ejected from the same element will emit an identical characteristic x-ray, which can then be quantified to determine the proportion of atoms from that element present in the sample (Murphy, 2010).

2.2.1 Portable XRF analysis

The XRF spectrometer purchased by Acadian Mining is an energy dispersive table-top X-5000 made by INNOV-X Systems. During each analysis three successive sets of 30kV x-ray beams are emitted, each lasting one minute. Characteristic x-rays are then identified by the silicon drift detector (SDD) which converts the radiation into voltage pulses that are quantified by the in-place multi-channel analyzer and displayed in chart and table form on the XRF's display screen. The XRF spectrometer analyzes for 49 elements (P, S, Cl, K, Ca, Ti, V, Cr, Mn, Fe, Co, Ni, Cu, Zn, As, Se, Rb, Sr, Y, Zr, Nb, Mo, Rh, Pd, Cd, Sn, Sb, Ba, La, Ce, Pr, Nd, Sm, Pt, Au, Hg, Pb, Bi and U). They are reported on a parts per million scale (ppm) and data can be exported from the device directly onto a USB drive in an Excel spreadsheet format.

2.2.1.1. Calculating and working with error

For each element analyzed, the XRF spectrometer calculates a region of error which is based on the duration of the measurement, as well as the quality of predetermined calibration standards (Murphy, 2010, Appendix C).

Attention was paid to the XRF spectrometer's precision by checking the precision of the data. Twenty samples were analyzed ten times each (see Table 1) to ensure that the XRF spectrometer produced unbiased and precise results, which was a method to see that the sample is homogeneous.

In addition, 30 samples were sent to SGS laboratories to undergo ICP-AES/MS, four-acid digestion analysis. The principle purpose for this was to calibrate the XRF machine, but it also helps to check the spectrometer's relative accuracy and the data integrity (Appendix A).

2.2.2 Calibration techniques

One concern regarding using an X-ray fluorescence spectrometer as the main method of geochemical analysis is that, although the results are reproducible, they are not necessarily accurate. To evaluate this, samples were sent to a separate laboratory to undergo ICP-AES and ICP-MS analysis to compare with data in this study. Although introducing comparison to ICP-AES/MS which has its own error and standards, this method (XRF spectrometry) is being

explored due to its low cost and fast results. The overall purpose of this study is to ensure that the XRF data is reliable

Thirty samples were selected and shipped to SGS Laboratories for ICP-AES and ICP-MS analysis. The samples were selected based on having a range of fine fraction gold grades, as well a range of trace element amounts. The analysis package chosen for SGS was ICM40B, which analyses 49 elements by four-acid digestion (Appendix A).

By assuming that the ICP-AES/MS analysis is more accurate (with a higher resolution), we can use the data to evaluate the accuracy of the XRF data and also calibrate the X-ray fluorescence data. This is done by plotting the elements of each analytical method against each other in bivariate plots to correct for any possible scaling differences.

2.2.3 Geochemical Analysis

Binary plots were created to determine the host-rock lithology, as well as to look for elements which has sampled that deviated from the host rock lithology pattern and therefore may represent alteration within the deposit. By predicting which elements may be mobile during hydrothermal alteration processes, elements were plotted against each other in binary diagrams in order to determine the elements which were least likely to be mobile during hydrothermal alteration. Where the bivariate plots had good correlation with each other and a nearly linear trend tested by correlation coefficients these elements were selected as best reflecting the host rock lithology and not having undergone hydrothermal alteration during the mineralizing events. This linear trend reflects the general lithological packages that are found within the Beaver Dam deposit. To use the whole rock geochemistry as a proxy for the mineral phases within the

deposit, these immobile elements which reflect the host rock lithology were plotted against elements hypothesized to have undergone alteration. If samples deviated from the trend of the host rock lithology (either elevated or depleted), it is concluded that they potentially underwent alteration. These elements which may show alteration were then plotted against the fine fraction of gold to determine any geochemical correlation between hydrothermal alteration and gold.

Drillhole cross sections were also created to determine if there was a spatial correlation between alteration and gold on a scale greater than the 1m sampling intervals. These sections consist of the analysis of the 1m intervals of samples taken from the full drill holes and have histograms on the concentrations of altered elements on one side of the drill hole, and concentrations of the fine fraction of gold on the other, to look for trends across the deposit.

When correlating concentrations of elements of interest with gold, an R^2 value has been calculated to help quantify the amount of correlation. R^2 is the correlation coefficient, whose values range from 0 to 1, and it predicts the proportion of variability within the data set (Evans, 1996). To calculate R^2, R (the measurement of the degree in which coordinates x and y are linearly correlated) must be calculated first, using equation 1.1 (Evans, 1996).

$$R = \frac{\sum_i [(x_i - \bar{x})(y_i - \bar{y})]}{\sqrt{\sum_i [(x_i - \bar{x})^2] \sum_i [(y_i - \bar{y})^2]}} \qquad \text{(Equation 1.1)}$$

An R^2 value ranging from 0-4% is considered to be statistically 'very weak', and a value greater than 36% is statistically 'strong' to 'very strong' (Evans, 1996).

3.0 Results

3.1 Introduction

As stated previously, the results of this study are a product of XRF analysis, and although the spectrometer used has been verified for relative precision and accuracy, the purpose of this study is to look for overall trends in relative abundance, and not necessarily absolute concentrations. In addition to determining geochemical and spatial associations between alteration with the gold mineralization at Beaver Dam, this study is testing the reliability of portable XRF devices as an inexpensive alternative for more expensive geochemical analysis.

Over 5000 samples were analyzed from over 50 drill cores located in the mineralized zone of the deposit. These data are proprietary and owned by Acadian Mining, but they have permitted the release of representative data which are compiled in Appendix A. Samples consist of pulverized drill pulp that was sampled at 1m intervals irrespective of lithology, quartz veining, or alteration. The sampling and analyses were done systematically down each full drill hole to determine the full extent and spatial distribution of alteration and mineralization. However, before this analysis can be done, it is important to ensure that the data is both reproducible, and relatively accurate, and therefore considered to be "good data".

3.2 Data Integrity

3.2.1 Accuracy of the data

To test the accuracy of the data, a subset of 30 samples were sent for ICP-MS analysis. By plotting the ICP-MS results against the XRF results (Appendix A), most elemental plots created linear trends with a slope close to or equal to one, and a high corresponding R^2 value Fig. 8). This good correlation confirms the relative accuracy of the XRF results to the ICP-MS data. Elements that had plots which deviated from the linear trend indicates either matrix error in the XRF data where the concentrations are detection limits, or where there is a peak overlap. Elements with weak correlations between the XRF and ICP-MS data were not used in further analyses. When some elements are in low concentrations (falling below the spectrometer's detection limits), sometimes their concentrations are reported as negative values.

Elements that had plots which deviated from the linear trend indicates either matrix error in the XRF data where the concentrations are detection limits, or where there is a peak overlap. Elements with weak correlations between the XRF and ICP-MS data were not used in further analyses. When some elements are in low concentrations (falling below the spectrometer's detection limits), sometimes their concentrations are reported as negative values. A portable XRF is intended to analyze elements with elevated concentrations in the field and therefore the calibration disk is generally elevated in many of the elements. Therefore, when a sample contains low concentrations, the errors increase exponentially and the concentrations for particular elements are sometimes reported as negative values. These elements include P, Y, U, Sb, Ni, Au, Mo, La, Ce, Cd, and Bi; and have been removed from the overall analysis as they are not reliable. Bismuth and Au XRF data were not used because of peak overlaps with Pb and As,

respectively. Although Y and Zr do not correlate well in binary plotes of the XRF data vs. the ICP-MS data, most likely the mineral phases in which these elements did not undergo full digestion during the sample preparation during ICP-MS analysis.

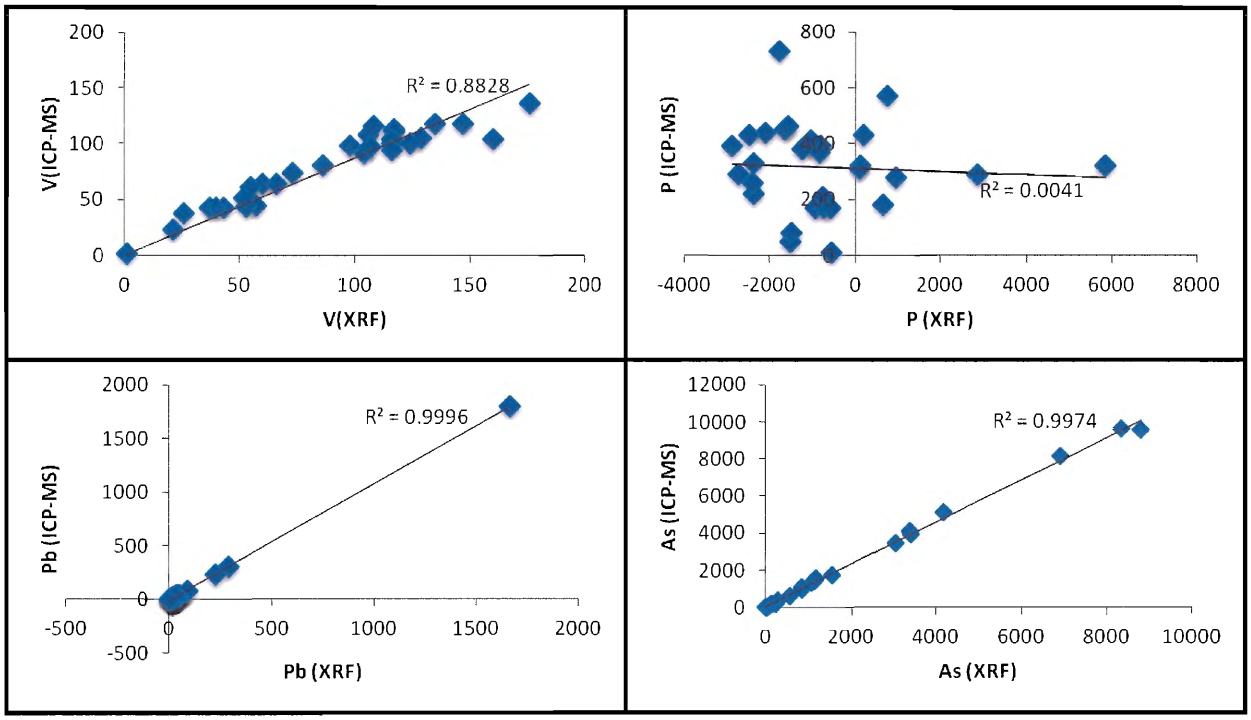

Figure 8. Representative plots of ICP-MS data vs. XRF data. (All data reported in ppm)

3.2.2 Precision of the data

To ensure that the XRF data are reproducible, 20 samples were arbitrarily chosen to be reanalyzed ten times each and subsequently undergo statistical analysis to determine the standard deviation and percent error of the analyses. Of the 49 elements which the XRF analyzes for, only 16 elements (displayed in table 1) were determined to be reproducible/ or that they were previously determine to not be usable due to their low accuracy (as shown with the ICP-MS

results in section 3.2.1), were in low concentrations, or had peak overlap. All 16 elements had a standard deviation falling within 1 σ of the mean, and a percent error lower than 3%. This suggests that the data that is used for this study are reliable and reproducible data and considered "good data" for the purposes of this study.

Table 1. Statistical analysis of the reproducibility of a subset of the XRF data

Elements	Mean (ppm)	Standard Deviation	Standard Error	% Error
S	4122.9	400.34	63.43	3.07
K	30939.4	667.49	218.58	0.68
Ca	19293.3	323.01	69.59	0.52
Ti	5153.5	91.44	31.19	0.56
V	96.2	3.11	1.07	1.02
Cr	78.6	3.33	1.66	1.34
Mn	879.3	17.44	4.86	0.62
Fe	52315.4	497.24	209.43	0.30
Co	20.35	1.23	0.28	1.92
Cu	39	1.88	0.53	1.52
Zn	83.3	3.68	0.78	1.39
As	16.38	25.36	6.69	0.48
Rb	102.54	1.24	0.42	0.38
Sr	160.3	4.29	1.91	0.84
Zr	184.3	4.42	1.64	0.75
Ba	433.9	10.08	3.98	0.73

3.3 Geochemistry and Lithology

3.3.1 General Lithologies

Element mobility most often takes place during weathering, diagenesis, metamorphism, or hydrothermal activity (Rollinson, 1993). The alteration that this study focuses on is related to the hydrothermal activity which is associated with the quartz veining and wall rock alteration which developed through fluid-rock interaction in multiple stages. The alteration that may have occurred during weathering, diagenesis and metamorphism is not addressed in this study, and so for our purposes, any of this alteration is considered to be part of the host rock geochemical signature. Through trial and error, multiple pairs of elements were plotted to first determine which elements were relatively immobile during hydrothermal alteration. The objective was to identify geochemistry that is reflective of primary lithologies irrespective of alteration through these immobile elements. Titanium, Cr, and V show very good linear correlation with little deviation from the slope, likely reflecting the host rock lithology. Figure 9 shows these immobile elements plotted against one another, as well as the representative average Phanerozoic quartz arenite and North American Shale Composite (NASC). The average Phanerozoic quartz arenite (Condie *et al.,* 1991) is a normalized average of elemental concentrations to minimize the effect of varying carbonate within the sample. The North American Shale Composite represents the average crustal material and represents normalized elemental concentrations from post-Archaean shale (Boryta and Condie, 1990).

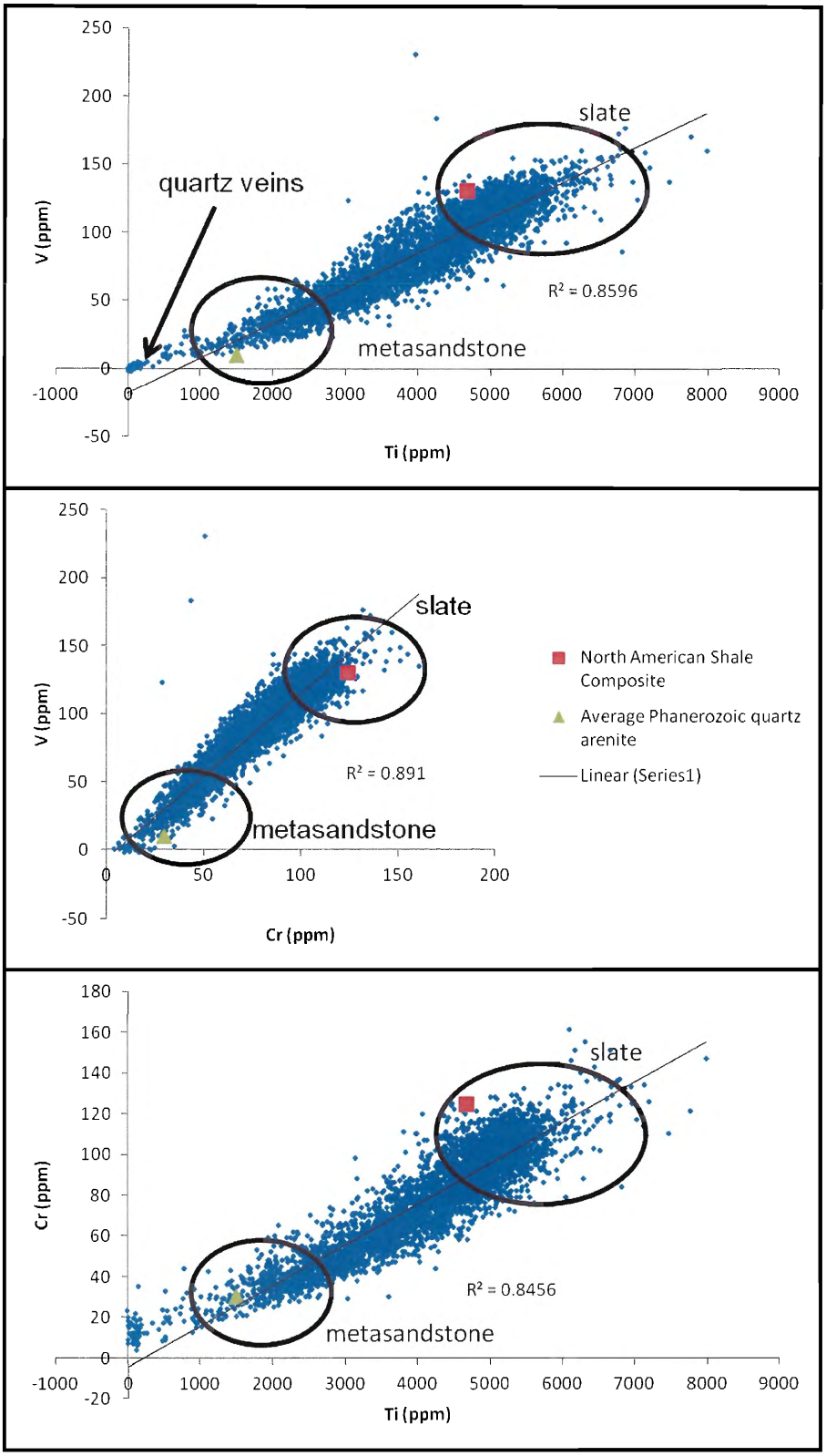

Figure 9. Elemental plots reflecting the host rock geochemistry of the Beaver Dam using transitional elements Ti, V, and Cr. General lithologies are highlighted (all values reported in ppm).

From historical drillhole logs, the broad lithological groups that comprise the Beaver Dam deposit include quartz veins, metasandstones, and slates. Figure 9 distinguishes these lithological groups, which are also generally distinguished by plotting the North American Shale Composite (NASC) and the average Phanerozoic quartz arenite. Pure quartz veins contain little to no concentrations of the transitional immobile elements Ti, Cr, or V, and therefore samples taken from quartz veins will plot near or at the origin in the plots in Figure 9. Metasandstones typically contain high silica contents, and relatively low concentrations of trace elements (V, Ti and Cr). In contrast, slates will contain higher concentrations of these trace elements due to the abundance of micas and clays within their composition. The trends shown in Figure 9, permit the subdivision of these lithologic boundaries, however due to the nature of the sampling process (samples were taken in 1m intervals, irrespective of lithology or alteration), as well as the presence of interbedded metasiltstone, there is a mixing zone between the three rock groups. This is why there is a continuous linear trend in these figures as opposed to distinct groups. Comparatively, Figure 10 is a plot of V vs. Zr, which shows an inverse relationship in these elements that reflect the concentration of detrital zircon in the coarser beds of metasandstone lithologies.

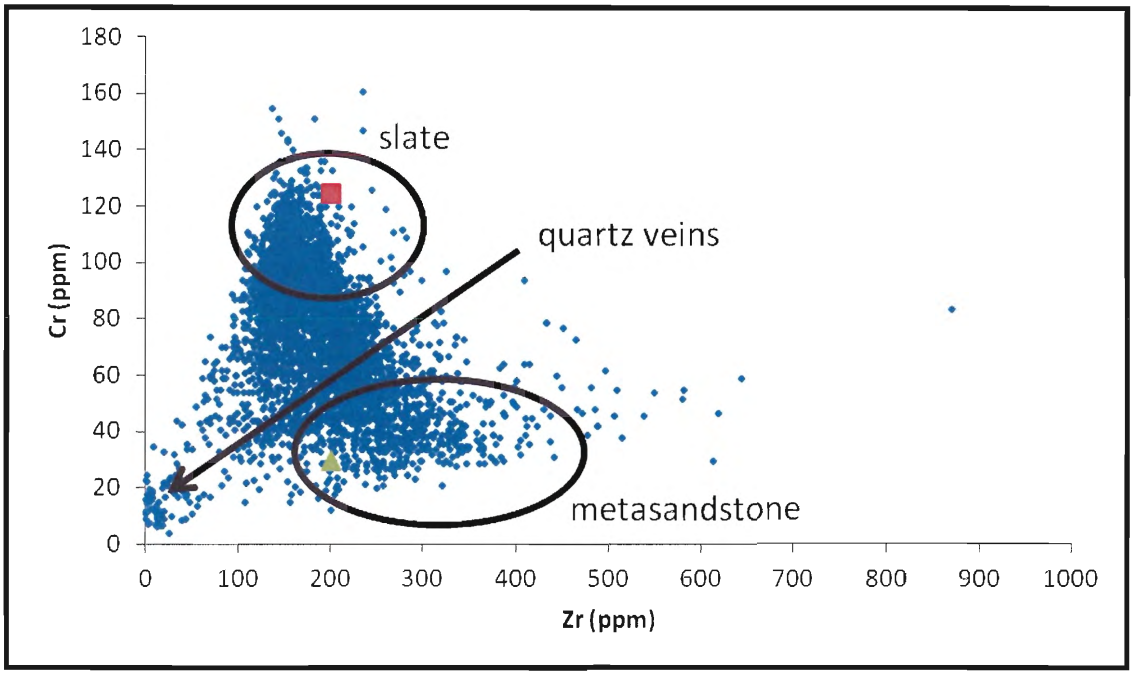

Figure 10. Inverse relationship between Cr and Zr reflecting detrital zircon concentrations in the coarser metasandstone rocks. The red square indicated the North American Shale Composite (NASC) and the green triangle represents the Average Phanerozoic quartz arenite to provide comparison. (all values reported in ppm)

3.3.2 Carbonate alteration

Binary plots were created to determine the general host-rock lithology, as well as to look for elements that yield anomalies that deviated from the host-rock lithological trend, which may represent hydrothermal alteration within the deposit. These elements were then plotted against the values from the fine fraction of gold to determine if any of these alteration indices are geochemically associated with gold.

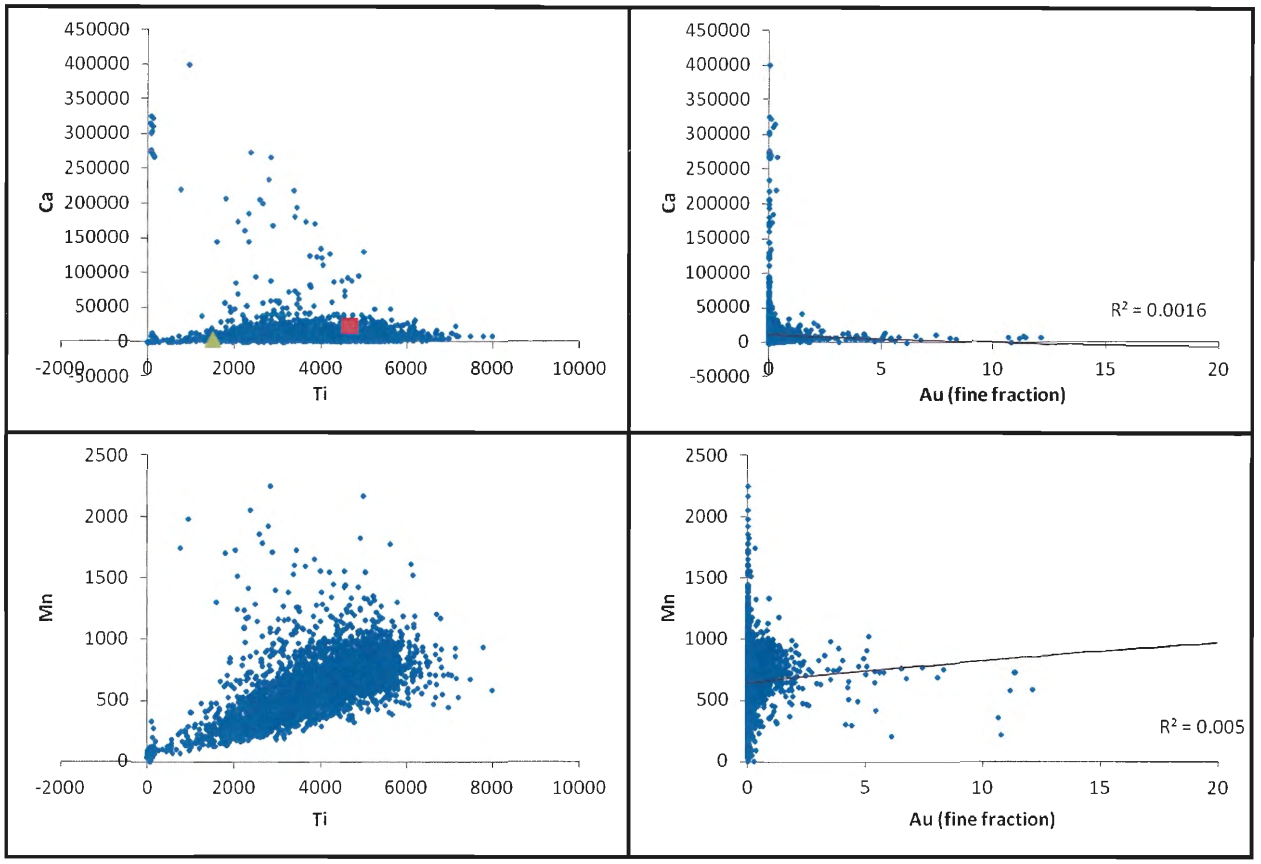

Figure 11. Calcium vs. Ti and Mn vs. Ti plots illustrating enrichment of Ca and Mn in some samples. This enrichment is likely due to the presence of carbonate associated with quartz veining. Also shown are plots of Ca vs. Au (fine fraction) and Mn vs. Au (fine fraction) illustrating their very weak correlation. The red square indicated the North American Shale Composite (NASC) and the green triangle represents the Average Phanerozoic quartz arenite to provide comparison. (all values reported in ppm)

To test for carbonate alteration, Mn and Ca were plotted against Ti and V shown in Figure 11. Some samples show elevated Mn and Ca concentrations relative to the overall host rock compositional trend. Typically, carbonate alteration is observed in the hanging wall of the Mud Lake Fault (Fig. 4), filling in late brittle faults as veinlets. This zone of faulting could have been a fluid conduit, and therefore the samples with anomalous Ca and Mn were plotted against the fine fraction of gold to determine if the carbonate alteration and gold mineralization are associated (Fig. 11). There is a very poor correlation between both the Ca and Mn relative to the fine fraction of gold, as seen through the calculated R^2 values of 0.0016 and 0.005, respectively.

3.3.3 Alkali/ Alkali Earth elements

Alkali and alkali earth elements are often associated with mobility during hydrothermal alteration (Rollinson, 1993). Potassium, Rb, Sr and Ba were plotted against Cr in order to determine if the alkali and alkali earth yielded concentrations that deviate from the host rock compositional trend (Fig. 12). Potassium, Rb, and Ba all show good correlations with Cr, likely reflecting the host lithology. Some samples show strongly enriched Sr concentrations relative to the host rock compositional trend. In particular, there is a cluster of samples with very low concentrations of Cr and high concentrations of Sr that can't be explained by lithology. A few samples of slate (higher concentrations of Cr) show slight depletion of Rb and Ba relative to the host rock geochemical trend (Fig. 12) also suggest local alteration.

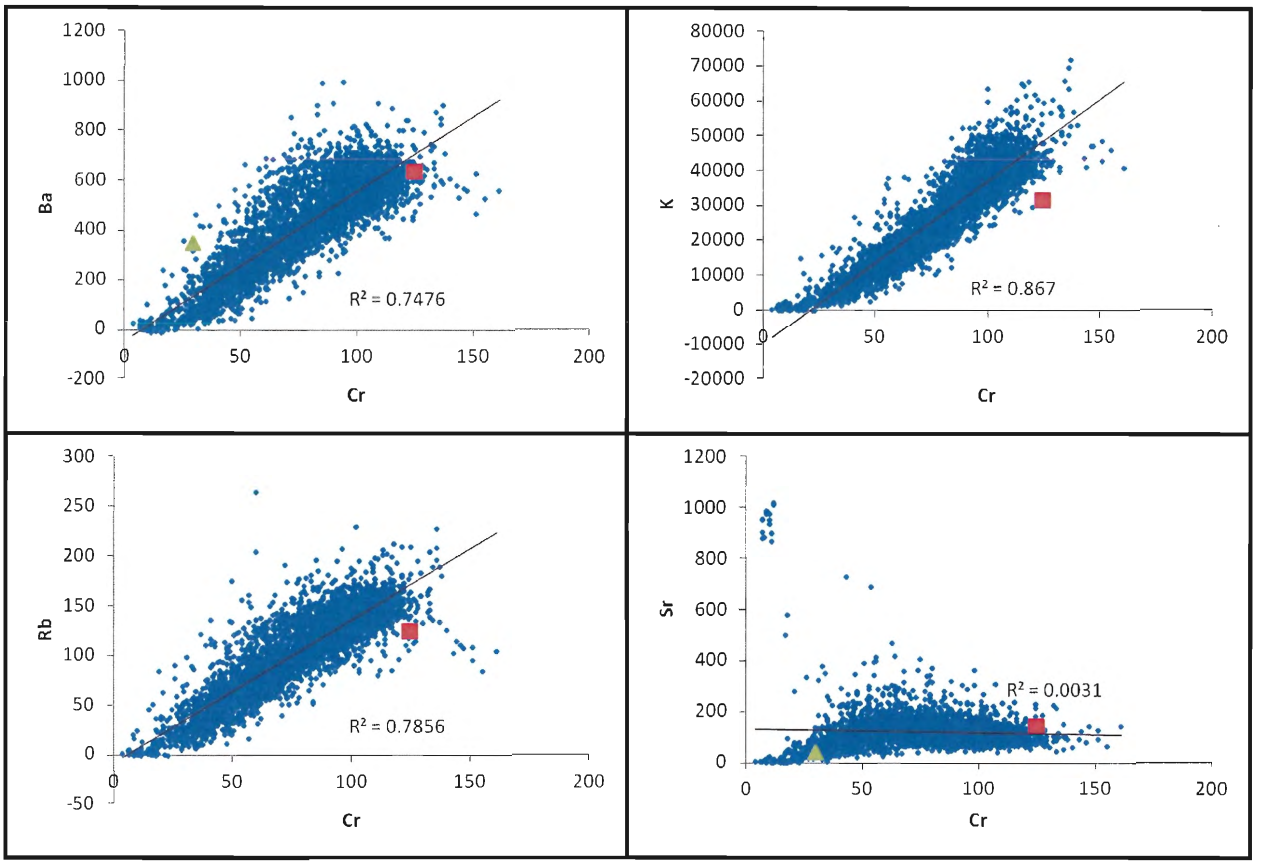

Figure 12. Binary plots of alkali and alkali earth elements Ba, K, Rb and Sr plotted against the immobile element Cr. The red square indicated the North American Shale Composite (NASC) and the green triangle represents the Average Phanerozoic quartz arenite to provide comparison. (all values reported in ppm)

3.3.4 Metals commonly associated with sulphide minerals

Other elements which were plotted against the immobile transitional elements include Fe, Cu and Pb. These elements occur in sulphide phases that were documented by Kontak and Smith (1993) to be related to hydrothermal alteration and therefore they were expected to show enrichment relative to the host rock geochemical signature (Fig.13). Iron shows good correlation with the transitional elements, with an R^2 value of 0.8738. When these elements (Fe, Cu and Pb)

are plotted versus the fine fraction of gold, they all show a very poor correlation with low R^2 values of 0.011, 0.0004, and 0.0606, respectively.

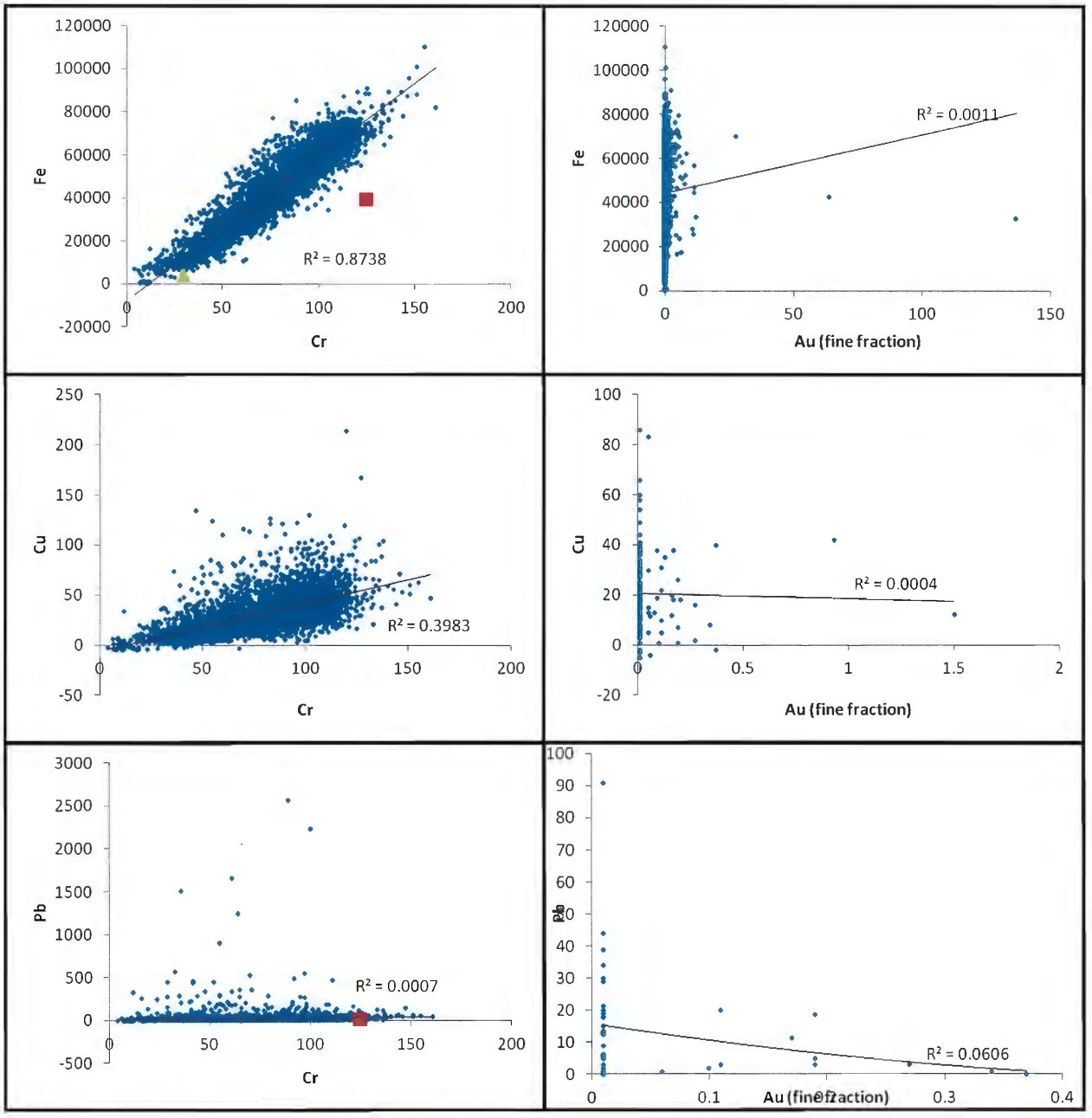

Figure 13. Binary plots of elements Fe, Cu, and Pb vs. the immobile element Cr as well as the fine fraction of gold. (all values reported in ppm)

3.3.5 Arsenic and zinc alteration

Elements which showed the greatest amount of mobility were As and Zn. Both As and Zn have a large number of samples which are significantly greater than the plotted NASC. These elements may be reflecting the presence of arsenopyrite and sphalerite which are observed within the deposit, however it is also possible that these elements are found as trace metals within the host rock geochemistry. Samples with anomalous As and Zn are plotted against the fine fraction of gold to determine if there is a correlation (Fig. 14). Arsenic shows a very weak correlation with gold, with a corresponding R^2 value of 0.0002. In addition, Zinc also shows a statistically very weak geochemical correlation with gold, with an R^2 value of only 0.0309. It is possible that there may be geochemical trends between alteration and gold on a scale greater than 1 m, and therefore cross sections have been generated to look for potential larger spatial correlations.

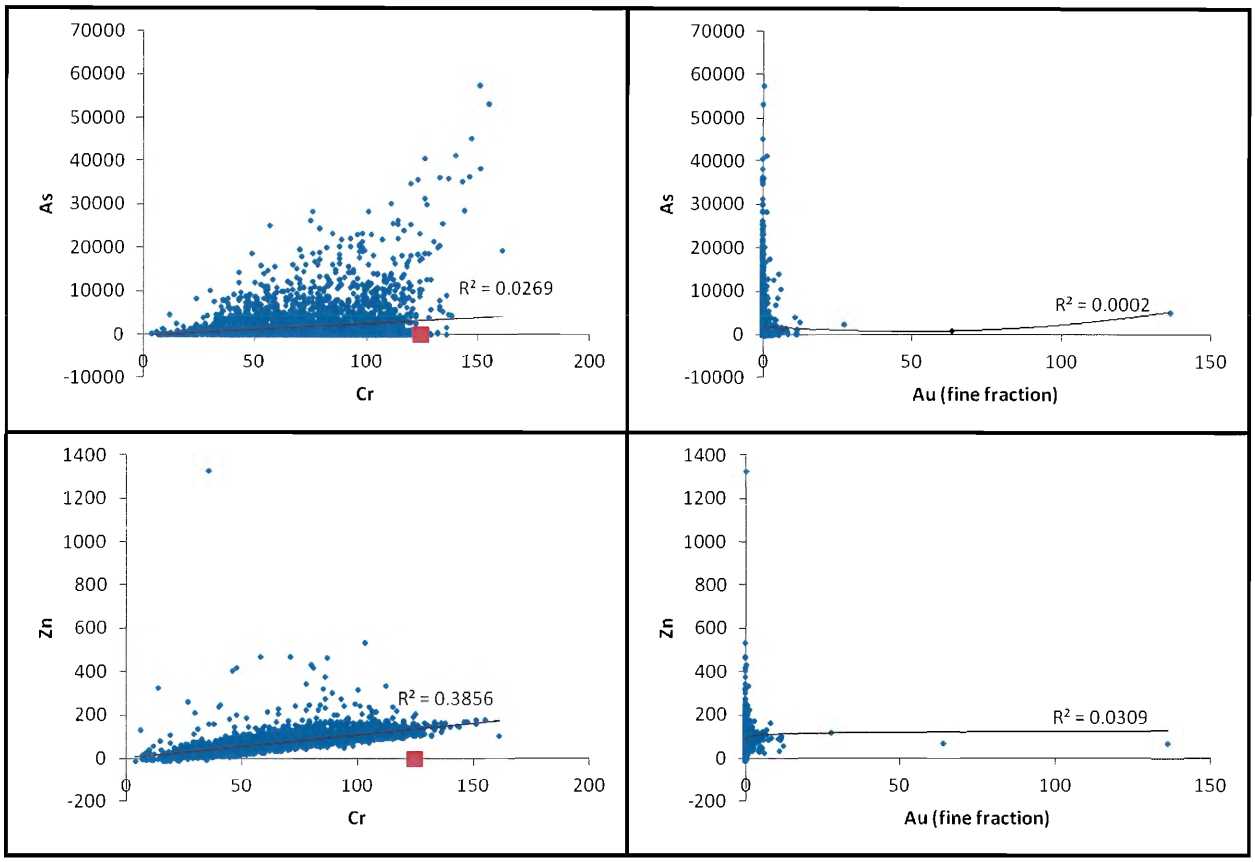

Figure 14. As and Zn versus both the immobile element Cr and the fine fraction of Au (all values reported in ppm)

3.4 Spatial Distribution

In general the above analysis indicated there is only minor evidence of alteration related to vein emplacement and related mineralization. In addition, there is poor correlation of gold with other elements. Regarding the latter is it noted that this non-correlation is based on comparison of individual samples and any spatial relation was not evaluated.

In addition to the geochemical analysis that was conducted, cross sections of the drill holes analyzed were generated, displaying the general lithologies of the deposit, as well as histograms of both the fine fraction of gold and elements which showed enrichment or depletion relative to the host rock geochemical trend (Figs. 15-18). This was done to determine whether

there is perhaps a spatial correlation between gold and alteration on a scale larger than the 1m sample intervals reflected in the binary geochemical plots.

A set of 13 sections have been generated from the main mineralized zone of the deposit (800E to 1100E, refer to Fig.15 and Appendix B). Each section contains drill holes that have been systematically logged, sampled at 1 m intervals and analyzed for Au by fire assay and whole-rock lithogeochemistry by XRF spectrometry. The concentrations of elements which may indicate the hydrothermal alteration, as well as the concentration of the fine fraction of gold are displayed as histograms down the hole in an attempt to determine whether there are any spatial relationships.

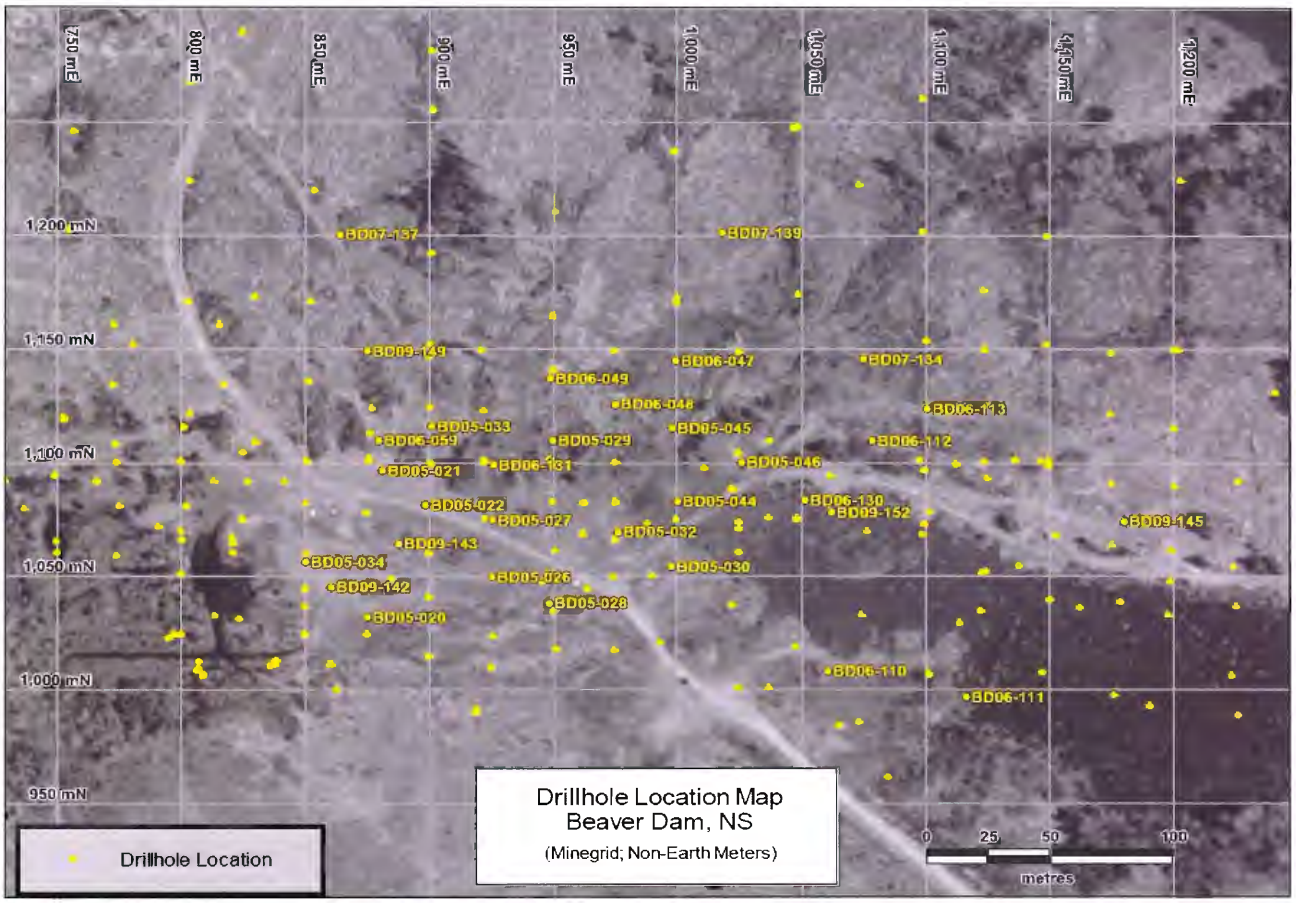

Figure 14. Beaver Dam drillhole location map of the main zone of mineralization. The cross sections in Figures 16-18 and Appendix B correspond to the mine grid easting lines

Elements with the strongest enrichment relative to the host rock compositional trends are Ca, As, and Zn, and these were selected to be plotted spatially against the fine fraction of gold in cross section. Calcium appears to partition into the metasandstones as a general trend, although there is a relatively wide distribution along drill holes; however there is no apparent correlation with the corresponding gold values (Fig. 16). Arsenic is concentrated in a zone documented in drill logs to be rich in arsenopyrite and the gold is distinctly structurally lower (Fig. 17). Both As and Zn appear slightly enriched within the Papke and Austen slate-dominated lithologic units (Figs. 17 and 18), which are also the zones where the majority of gold is documented, although there is no close correlation with gold values. These spatial sections all suggest a spatial non-correlation between gold and these altered elements.

Additional cross sections were generated comparing gold values with K, Mn, Rb and Sr (Appendix B). As expected, Mn and Sr both have similar trends to Ca most likely because these three elements substitute for each other in carbonate alteration. Potassium and Rb both partition into the Papke and Austen slate-dominated lithologic units, which corresponds to the geochemical analysis.

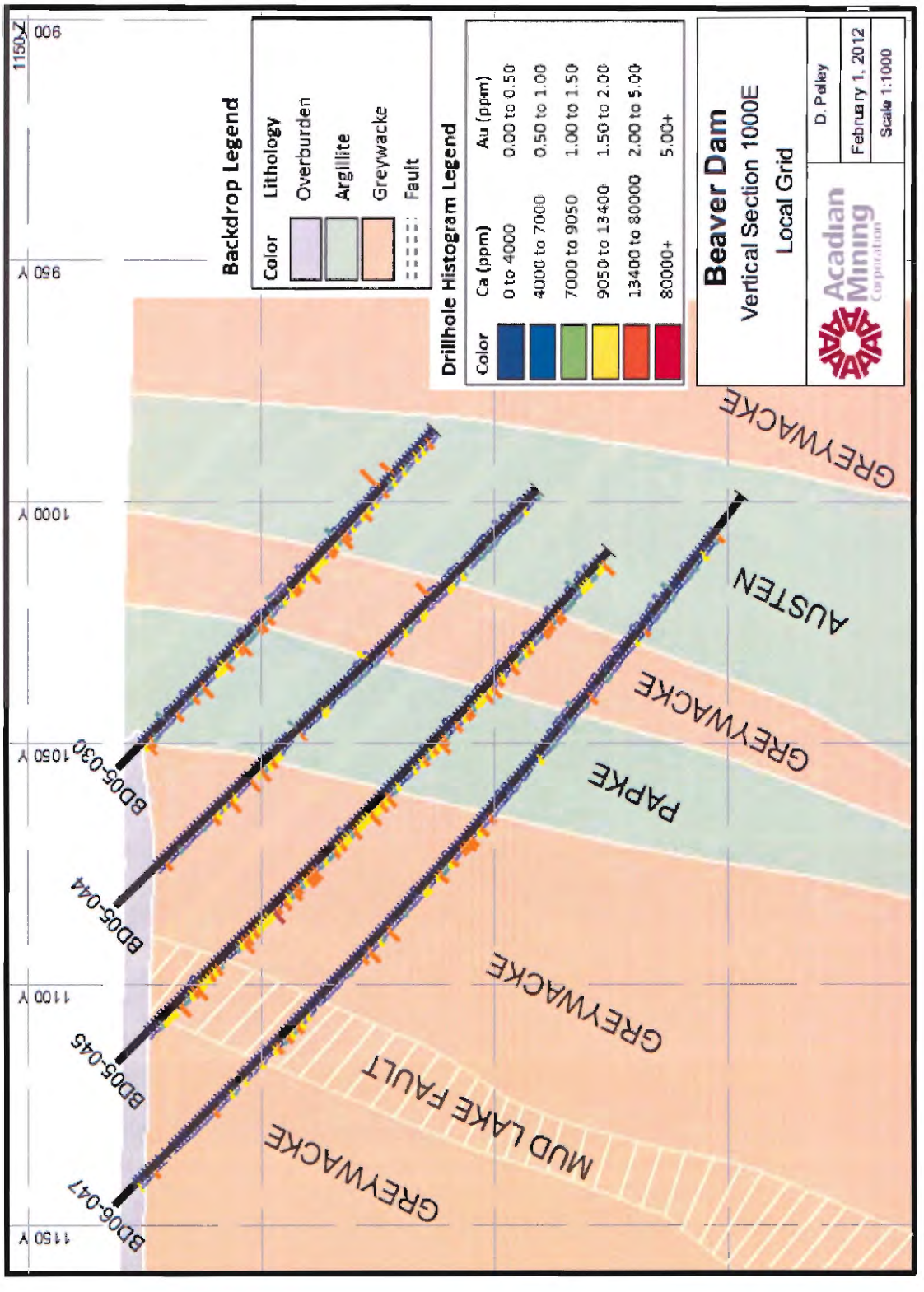

Figure 16 Representative cross section along line 1000E showing histograms of Au and Ca. Gold histograms are shown on the upper side of the drill hole trace and Ca histograms are shown on the lower side of the drill hole trace.

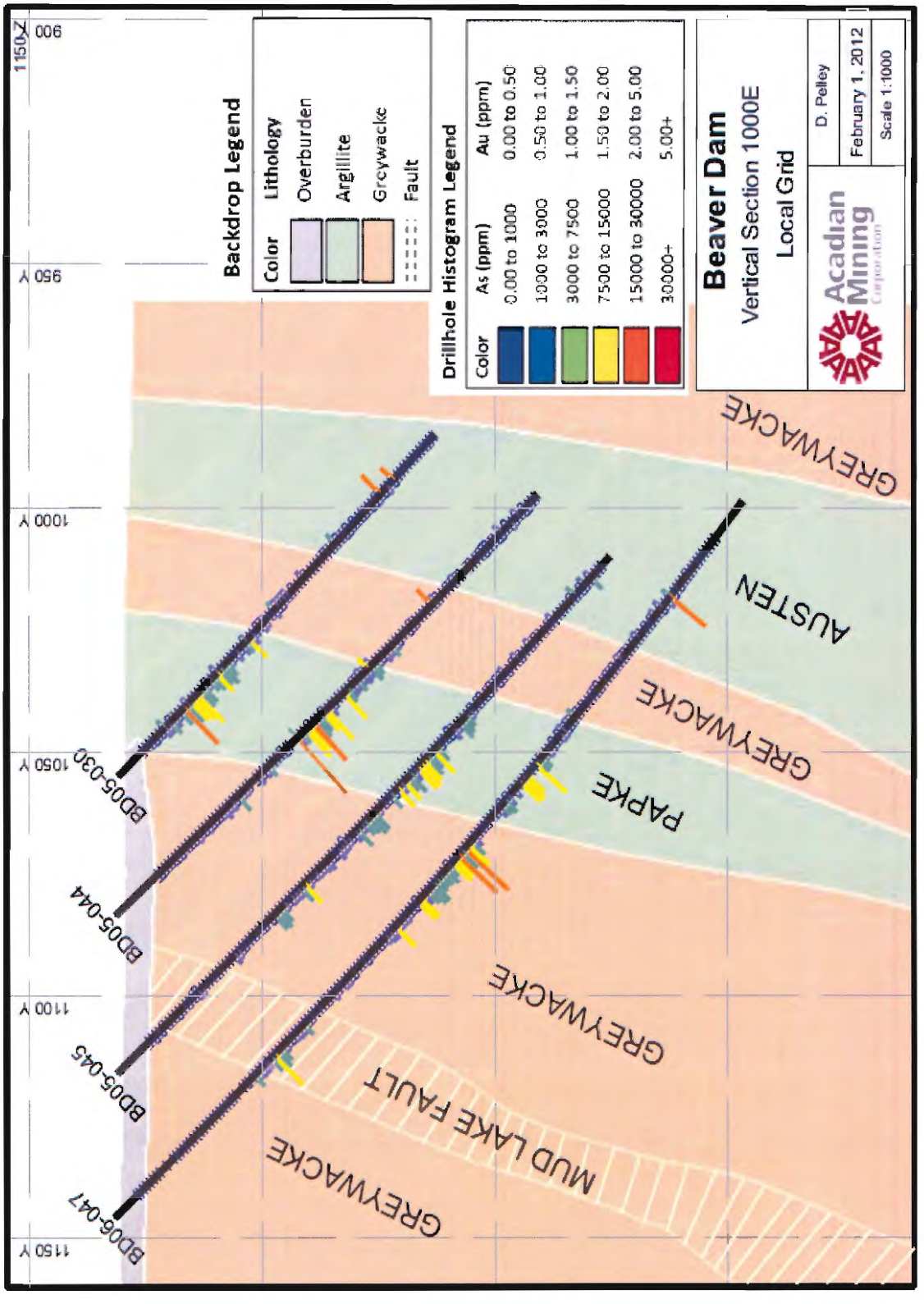

Figure 17. Representative cross section along line 1000E showing histograms of Au and As. Gold histograms are shown on the upper side of the drill hole trace and As histograms are shown on the lower side of the drill hole trace.

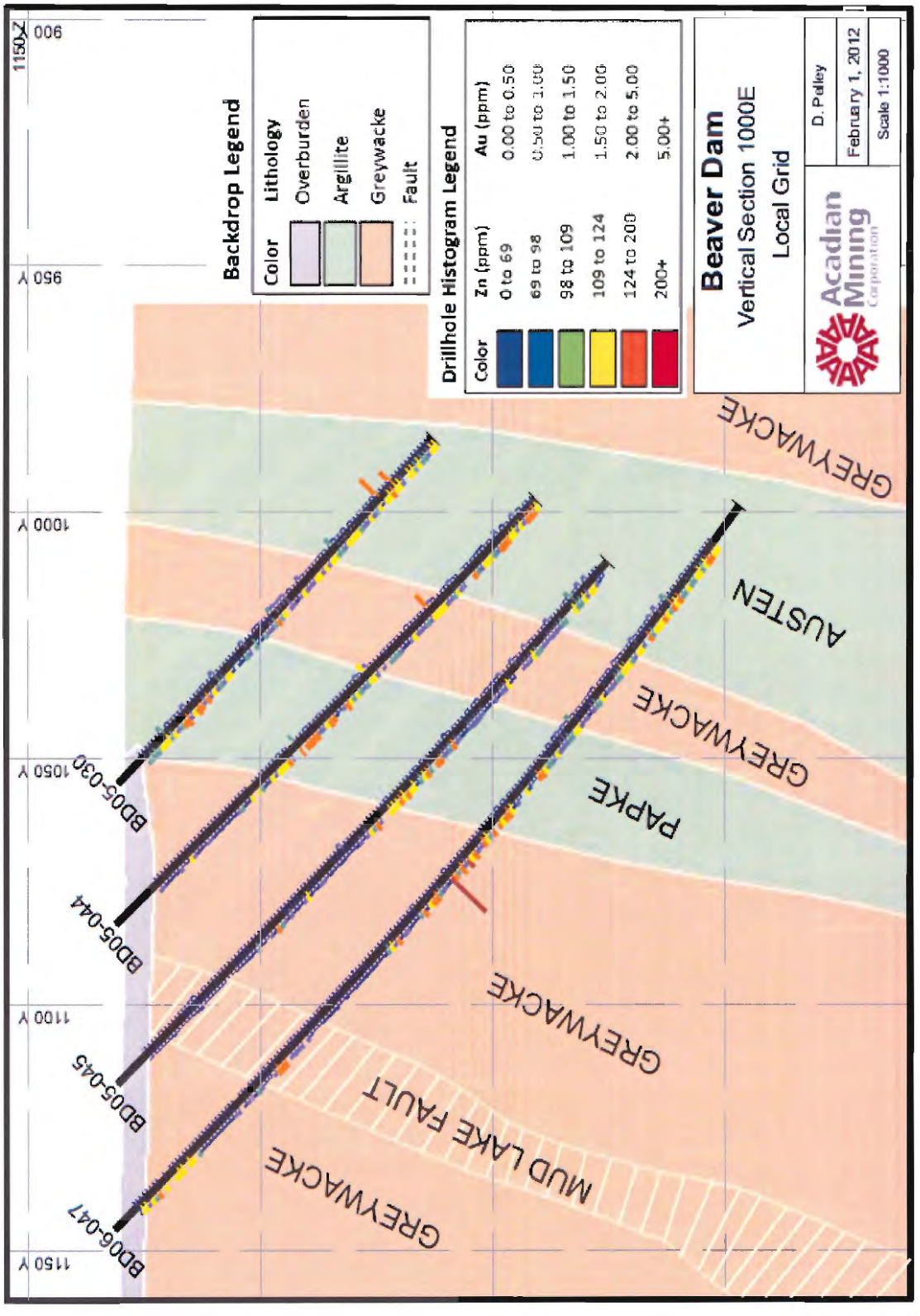

Figure 18. Representative cross section along line 1000E showing histograms of Au and Zn. Gold histograms are shown on the upper side of the drill hole trace and Zn histograms are shown on the lower side of the drill trace.

Cross sections comparing As to elements which may indicate hydrothermal alteration have also been generated in attempt to determine which of these elements may be paragenetically related with arsenic. Cross sections which compare values of As vs. Fe, Cu, K, Mn and Rb do not show any tangible correlation with arsenic (Appendix B). As the geochemical analysis indicated, Fe, K, and Rb all show partitioning into the Papke and Austen slate-dominated lithologic units, and therefore follow the host rock geochemical signatures. Manganese does not correlate well with As, but instead has a similar distribution to Ca and Sr. Copper is found in small concentrations and has a similar spatial distribution to Zn, however no correlation with As is evident. Although Zn seems to have many sample which are elevated in comparison to the host rock geochemical signature, cross sections show that Zn is controlled more by lithology than alteration.

4.0 Discussion

4.1 Introduction

By constructing bivariate plots of the concentrations of numerous elements determined by portable XRF spectrometry within the Beaver Dam deposit, some plots produce linear trends likely reflecting the composition of the host rock lithologies. In contrast, other samples which yielded higher or lower concentrations in comparison to the host rock lithological geochemical signatures may reflect hydrothermal alteration. The original scope of this study was to identify specific elements introduced during hydrothermal alteration which have compositional enrichment or depletion commensurate with Au grades, and therefore provide an additional exploration strategy. However, upon analysis, the data collected during this study reveals an apparent disassociation, or non-correlation, between hydrothermal alteration and gold. There are numerous possible reasons why there is an apparent non-correlation and some of them are discussed below as well as recommendations for future work in order to mitigate against potential flaws in the methodology of a study of this nature.

4.2 Accuracy and Precision

Ensuring that the XRF data is both accurate and precise is essential in order to be able to confidently interpret any data that is obtained. As previously stated, a subset of 30 samples (Appendix A) was analyzed both by XRF spectrometry as well as ICP-MS in order to compare results. Many elements correlated very well to the ICP-MS data, and are therefore considered to be accurate for the purpose of this study. Elements which did not correlate well to the ICP-MS data are considered unreliable due to their low detection limits by XRF, and cannot be used in

this study. Yittrium and Zr are exceptions to this rule, as they did not undergo full digestion in ICP-MS sample preparation.

Another subset of samples was taken and reanalyzed multiple times by XRF spectrometry to determine the statistical precision of the data. Sixteen of the elements which the XRF spectrometer analyzes for yield a percent error lower than 3%, and all of this data falls within 1 standard deviation of the mean, therefore the data is considered to be reliable for the purpose of this study.

The quality assurance and quality control procedures that were followed in this study has produced results which ensure that the energy dispersive XRF used here provide great numbers for the 16 elements which were ultimately used for analysis. This analytical method allowed for a large amount of data to be produced in a relatively quick and cost effective manner.

4.3 Bivariate plots

Binary diagrams have been generated to explore geochemical relationships in the Beaver Dam deposit. The initial purpose of this study was to look for pathfinder elements associated with gold to develop a more detailed description of gold mineralization in the Beaver Dam deposit. However, upon evaluation of the geochemical analysis, it appears that there are no trace elements which show any good correlation with the fine fraction of gold. Instead, the XRF data reveals geochemistry that is strongly controlled by the host-rock lithology (which includes the primary sediments of greywacke, shale, and metamorphism).

4.3.1 Host-rock lithology

Through trial and error, binary plots were made, looking for linear trends with little to no deviations from the slope to look for elements which may have been immobile within the deposit. Elements Cr, V, and Ti all show excellent correlation with eachother, and were therefore determined to represent the host rock lithology. When plotted against each other, Ti, Cr, and V have an average R^2 of 0.8654, which is a statistically very strong correlation, and provides confidence in the interpretation that these trends reflect a real geologic process. This geological signature has been interpreted to represent two of the main lithologies present in the deposit. Slates will concentrate transitional elements, which concentrate in micas and clays within their composition. Metasandstones are silica rich, and have low concentrations of Ti, Cr, and V relative to slate. Pure quartz veins are also interpreted to be nearly pure silica (and therefore nearly no concentrations of transitional elements) and will therefore be found near the origin. Zirconium is also a good proxy for the host rock lithology, as it concentrates within the metasandstones (in contrast to Cr, V and Ti).

4.3.2 Alteration

Bivariate plots which show samples with elevated concentrations relative to the geochemical signature of the host rock lithology are considered to have potentially undergone hydrothermal alteration. Through trial and error, many elements have been plotted against the previously determined immobile elements to look for potential proxies for alteration.

Calcium and Mn both yielded samples which deviated from the regression, which could indicate the presence of the aforementioned carbonate alteration which has been described

throughout the deposit. It is likely that Ca, Mn, and Sr all substitute for each other in carbonate phases. In the Ca vs. Ti plot, there are samples with anomalously high concentrations of Ca with little to no Ti, likely reflecting the thick quartz- carbonate veins. To determine the association between the carbonate alteration with the fine fraction of gold, both Ca and Mn were plotted against gold and they both showed a very weak correlation, suggesting that Ca and Mn were either introduced as separate events, or that gold underwent a later remobilization.

Alkali and alkali earth elements (Ba, Rb, K, and Sr) were also plotted against the immobile Cr in order to determine enrichment or depletion relative to the host rock geochemistry. Strontium shows a similar pattern to Ca, as they are of similar atomic size, and therefore Sr substitutes for Ca where carbonate is present during carbonate alteration explaining their similar geochemical signature. Barium, Sb, and K all had a geochemical signature that had a little deviation from the host rock geochemical signature, however they all have some samples which show a slight depletion of these elements in the slates, which could reflect quartz veining, or during wallrock/clay alteration. Overall these elements primarily reflect the host rock geochemical trend, with very weak alteration.

Because the presence of sulphides are often used as a proxy for gold, Fe, Cu, Pb, As, and Zn were all plotted against Cr in order to identify samples enriched in these elements relative to the geochemical signature of the host rock lithology which may reflect the presence of sulphides. Many samples showed higher concentrations relative to the host rock geochemistry (as well as their corresponding averages of the NASC and average Phanerozoic quartz arenite), however, when these samples showing the anomalous concentrations were plotted against the fine fraction of gold, they all yielded a very weak correlation, indicating that they were either introduced into

the system separately, or that the gold underwent a later stage of remobilization at a lower temperature (in which remobilization of sulphides would not have been possible).

In an attempt to look for general patterns within the geochemistry, plots of the major elements of interest were made to summarize the data (Figs. 19, 20). Figure 19 is a summary diagram for hole BD05-044 (Fig. 15), and provides a good comparison of both the geochemical and spatial distribution of the concentrations of the major elements of interest, including gold. The major lithologies (metasandstone and slate) are represented by colour, with quartz veins (in red) inferred from the geochemical spikes of gold anomalies. Chromium is meant to reflect the geochemical signature of the host rock lithology, and K and Zn both have a very similar geochemical pattern, and can therefore be interpreted to reflect the host rock lithology as well. Spikes within the Au signature may represent their presence within quartz veins, and we would expect to see spikes of Zr representing quartz veining as well since zirconium concentrates in silica rich lithologic groups. Calcium seems to partition within the metasandstones, which was also apparent within the cross sections that were generated (possibly reflecting brittle fractures and calcite veining). Arsenic shows a very interesting geochemical signature, where elevated arsenic is concentrated at the structural top of an approximately 40 m thick slate package. This abrupt signature may reflect hydrothermal alteration, although it does not strongly correspond to the gold values, so the timing of the two may still differ. In summary, many of the trace elements which have been analyzed show a strong correlation to the host rock geochemical signature, and hydrothermal alteration is generally weak, and poorly represented in this data.

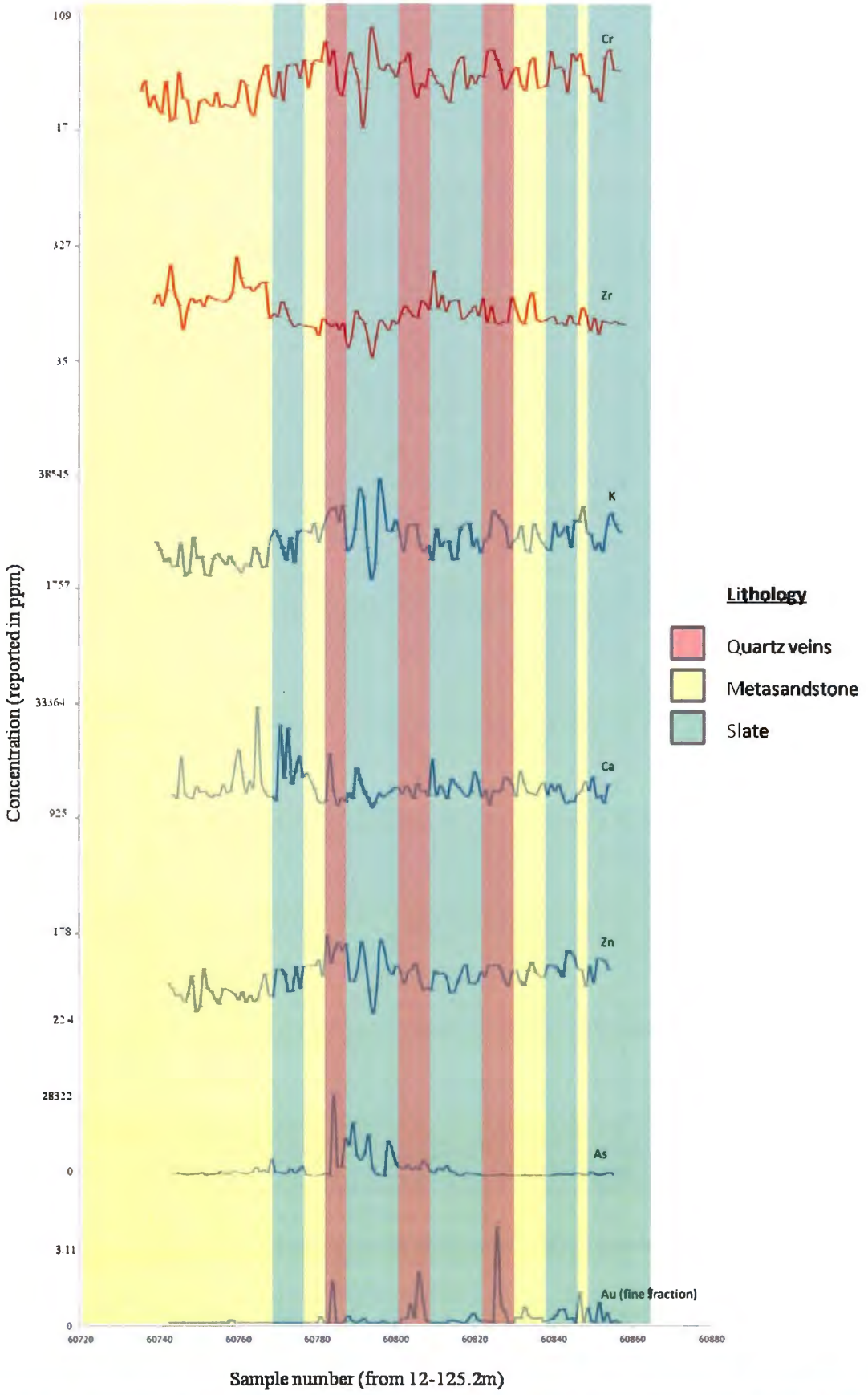

Figure 19. Summary diagram for drill hole BD05-044 (refer to Fig.15) plots the concentrations (in ppm) of the elements of interest: Cr, Zr, K, Ca, Zn, As and the fine fraction of Au. Each sample number represents 1 m intervals, and therefore the geochemical profile spans approximately 120 m. Background colours indicate lithology: yellow is a metasandstone and green is slate. Quartz veins (in red) are inferred by the spikes in concentration for Au.

Figure 20 is a summary diagram for drill hole BD05-030 (Fig. 15). Concentrations of Cr were used to represent the host rock lithology in the hole. Higher concentrations of Cr are generally found within the slate packages (the Papke unit is structurally higher than the Austen), and K and Zn both show a very similar geochemical signature, indicating that they both are controlled primarily by the host rock lithology. Calcium seems relatively evenly distributed, with potentially slightly higher elevations within the metasandstone unit, possibly reflecting brittle faulting and calcite veining as observed within the deposit. Quartz veins are inferred where there are significant spikes in concentration for the fine fraction of Au. Interestingly, where one of these spikes occur, there is also an observed negative anomaly in Cr, Zr, K, and Zn, which would further indicate the presence of a pure quartz vein. Elevated As is concentrated at the structural top of the Papke slate unit in both of these summary diagrams, and is relatively depleted within the rest of the section. This uneven distribution could indicate that As is a product of alteration, although it does not correlate with the gold values.

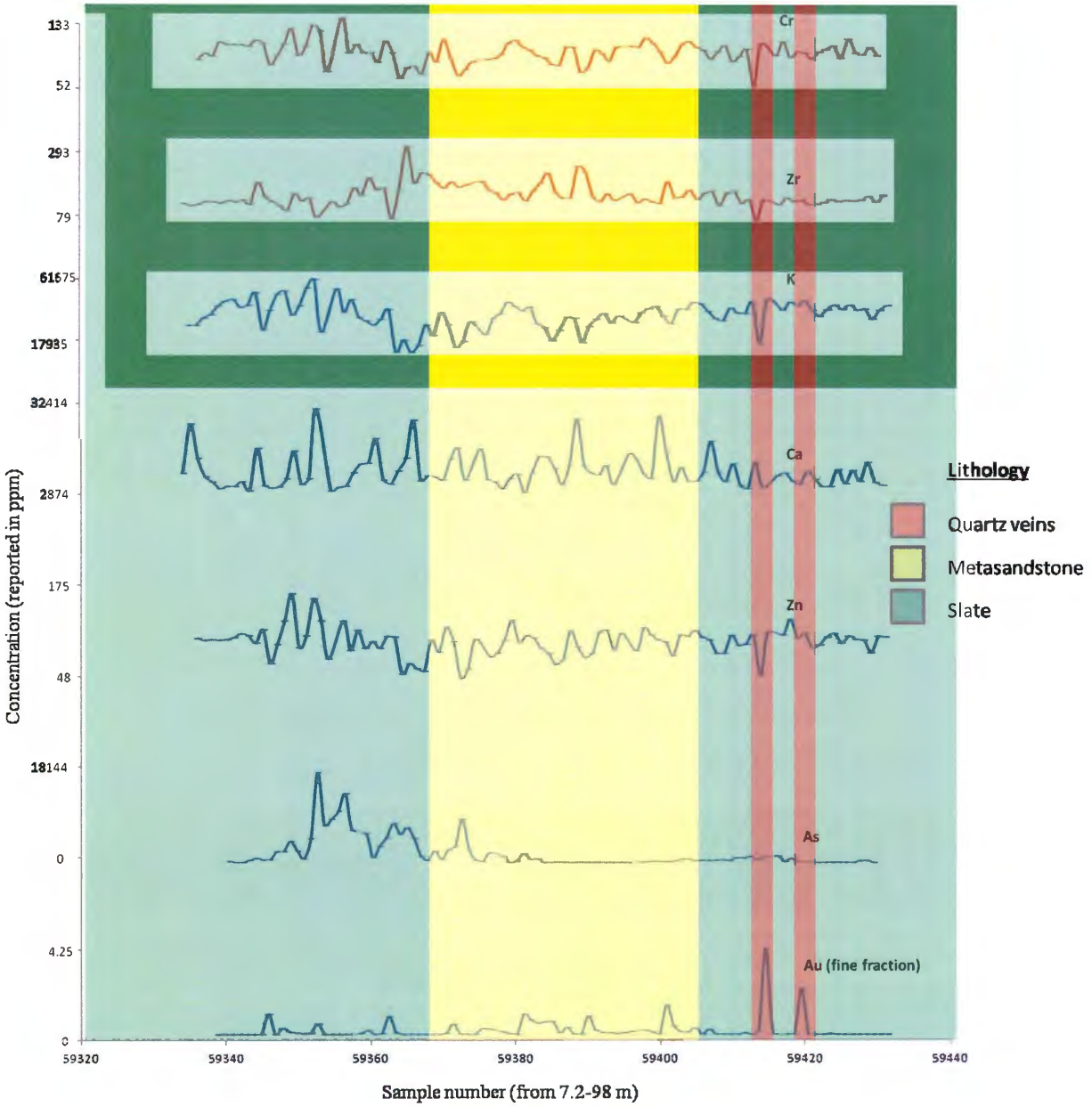

Figure20.Summary diagram for drill hole BD05-030 (refer to Fig.15) plots the concentrations (in ppm) of the elements of interest: Cr, Zr, K, Ca, Zn, As and the fine fraction of Au. Each sample number represents 1 m intervals, and therefore the geochemical profile spans approximately 91 m. Background colours indicate lithology: yellow is a metasandstone and green is slate. Quartz veins (in red) are inferred by the spikes in concentration for Au.

4.4 Spatial distribution

Sets of 13 spatial sections (Figs. 16-18, Appendix B) were generated to represent the main area of mineralization to look at spatial trends of elemental distributions compared to both the concentrations of gold and arsenic. Arsenic is concentrated in zones which are structurally higher than Au. This could indicate the presence of arsenopyrite located in the foot wall of the Mud Fault, or infilling brittle faults along this structurally higher region. Although it is possible to distinguish some partitioning trends of some elements into the host rock lithologies, there seems to be no correlations between any of these elevated elements relative to the gold. Elements Ca, Ba, Fe, K, Mn, Rb and Zn partition into lithologic zones of the drill holes, indicating that their concentrations partition and reflect the host rock lithology. These elements are widely distributed with no large anomalous spikes, which may indicate that these elements were not subject to hydrothermal alteration (or weakly associated with hydrothermal alteration), and are therefore reflecting the host rock lithology.

4.5 Issues with sampling protocol

As previously mentioned, sampling of this deposit was done before this study had taken place, and is not ideal for the scope of this study as lithologic contacts were not honoured. Drill core was sampled at 1 m intervals irrespective of the lithology, quartz veining, or hydrothermal alteration. This protocol has resulted in the mixing of lithological types and quartz veining which yields mixing zones between the lithological groups, and potentially dilutes the data. This sampling problem is worth mentioning, as it could potentially be the cause for these weak to non-correlations present in the geochemical analysis. Further work for this study would include a

sampling protocol that was done systematically based on lithology, quartz veining, and alteration to help distinguish patterns from the current problem of the mixing zones created. That said, there are very good correlations in plots of Ti vs. Cr, etc., which reflect the composition of the host rocks. From the data at hand, preliminary conclusions are still able to be derived.

Other potential causes of this apparent non-correlation between hydrothermal alteration and gold mineralization could include the very low degree of hydrothermal alteration present in the Beaver Dam deposit (essentially limited to silica flooding and a small amount of carbonate alteration). Additionally, gold commonly occurs as isolated nuggets and therefore the gold grade values determined from sampling drill core could be artificially enriched or depleted relative to the overall gold budget. Although measures were taken to avoid the nugget effect (by using duplicate Au analyses of the fine fraction of the sample pulps), it is still possible that there are still sub-100 micron nuggets present in the geochemical analysis, or that the large nuggets may have been pulverized to less than 100 microns. The nugget effect is a problem for geochemical interpretation because it will yield high variations of gold concentrations in each sample taken, no matter how close or systematic the sampling is done, and therefore the data are independent and it is not possible to draw reasonable geochemical trends (Dominy *et al.*, 2002). Using the fine fraction of the sample pulps is done to decrease the nugget effect, and ideally provide less erratic results, however it is possible that the gold grades are not representative. Additional bivariate plots were generated comparing alteration with the total gold concentrations (which includes both the coarse and fine fraction), however these weak correlations are still evident.

4.6 Possible paragenetic sequences

A geochemical non-correlation between elements indicating alteration and gold could indicate two paragenetic possibilities: 1) either that gold was introduced into the system as a separate fluid event, or 2) that gold was introduced into the deposit synchronously with the sulphides (most specifically aresenopyrite) during a high temperature phase, and then subsequently remobilized during a later, lower temperature fluid event.

Kontak and Smith (1993) infer that the temperature of vein formation (as summarized in Chapter 1.2.3) for the Stage I mineralogy was approximately 525°C and for Stage II mineralogy was approximately 375°C. Arsenopyrite is thought to have been synchronously deposited with the Stage II mineralogy, although paragenesis of the sulphides is poorly constrained. Kontak and Smith (1993) observed gold inclusions in arsenopyrite and pyrrhotite, and suggested that gold was not introduced as a separate event, but rather in conjunction with the sulphide minerals. Gold is a siderophile element, which is commonly associated with pyrite and arsenopyrite (Rankama and Sahama, 1950). Native gold is very chemically inert, and so it is possible that the gold underwent later remobilization (after Stage II mineral paragenesis) at temperatures below perhaps 200°C, where sulphide remobilization would not have been possible.

Further work could look for more gold inclusions within the arsenopyrite or other sulphide minerals, as well as to use electron microprobe analysis to look for gold inclusions within the chemical structure of these sulphide minerals. Such associations would confirm that the gold and sulphide mineralization were deposited synchronously, and the geochemical non-correlation that this study has found would further indicate that gold has indeed undergone a separate later phase

of remobilization at a lower temperature. Analyses to determine the temperature of formation of the gold grains could also be implemented to verify if this remobilization may have occurred.

5.0 Summary and Conclusions

This study used whole rock lithogeochemistry to determine if there is a geochemical or spatial correlation between alteration and gold in the Beaver Dam deposit, Nova Scotia. Samples which had been previously obtained by standard drillcore sampling methods by Acadian Mining have undergone energy dispersive XRF spectroscopy as an alternative to other geochemical analyses because it is both cost and time effective. Because the sample pulps were obtained prior to this study, the sampling protocol that was implemented has provided potential limitations for the interpretation of the data. A subset of the samples were analyzed by ICP-MS to ensure the precision of the data, and an additional subset of samples were reanalyzed to determine the statistical reproducibility of the data. Although some elements had to be discarded from this study due to their unreliable results, 16 have yielded good precise and reproducible results to allow for the interpretation of deposit scale trends in Beaver Dam's geochemistry.

The samples were taken irrespective of lithology, quartz veining, or alteration, and so a mixing zone is evident in the geochemical analysis, however because the host rock geochemical signature makes such strong correlations, preliminary conclusions were drawn. Titanium, V and Cr were determined to be immobile, and showed excellent correlation with each other that reflects the general composition of the host rocks in the deposit. Transitional elements Ti, Cr and V will generally partition into the slates, and are depleted in silica-rich metasandstones

which is reflected in the bivariate plots. Quartz veins are also evident in these binary plots as being comprised of almost entirely quartz (and therefore little to no trace element concentrations) and can be found near to the origin in these plots. The linear trend of these lithological plots represents a mixing zone between the metasandstone and slates, which represents both the interbedded nature of the deposit, and also may represent the sampling method previously described.

These transitional metals were then used as a proxy for lithology, and when plotted against other trace elements, samples which deviated from the linear correlation may potentially represent hydrothermal alteration within the deposit. The samples enriched above the host rock composition were subsequently plotted against the fine fraction of gold to determine any geochemical correlations; however all of these elements were not correlated to gold.

Cross sections were then generated to determine if there were relationships between alteration and gold on a larger scale, however no such relationships were found. Most elements in cross section had a wide distribution and represent the host rock geochemical signature. Arsenic had anomalous spikes in concentrations, which may represent hydrothermal alteration, however its abundance was structurally higher than the fine fraction of gold.

These lack of correlations between gold and potential alteration elements could be a product the non-ideal sampling method that was implemented, which may have resulted in a dilution of the data. In addition, it is possible that the fine fraction of gold that was used either did not extensively sieve out all gold 'nuggets', and so gold grade values determined by fire assay may be artificially enriched or depleted. Additionally, because the degree hydrothermal alteration

observed in the Beaver Dam deposit is so low and somewhat limited to silica flooding and minor carbonate alteration; geochemical signatures may be very small and difficult to distinguish.

Due to the fact that plots of the transitional elements Ti, Cr, and V create very good correlations with eachother, it seems very likely that these elements represent the host rock lithology in Beaver Dam, and therefore from the data at hand, it is possible to derive some preliminary conclusions. Potential reasons that explain this geochemical non-correlation lead to the hypotheses that gold was either 1) introduced as a separate fluid event within the deposit, or 2) that gold was deposited synchronously with the stage II mineralogy and subsequently underwent a later, lower-temperature remobilization. The latter hypothesis seems to be more likely, since earlier studies have observed gold inclusions within arsenopyrite, indicating that the sulphide minerals were deposited with the gold.

The confidence in the geochemical analysis for this study could be obtained by initiating a new sampling method in which samples were taken systematically targeting main lithologies, quartz veining and alteration. This would ensure that the geochemical interpretation solely reflects that of the deposit, and no dilution in the data would occur. If further geochemical analysis yields these similar non-correlations between alteration and gold, further work could be done to determine the paragenesis of gold in the deposit. If the gold has undergone remobilization, the temperature of the gold remobilization could be determined, as well as to look for more gold inclusions in association with the sulphide minerals, or within the chemical structure of the sulphide minerals.

Appendix A:
Representative XRF, ICP-MS, and gold assay data

A subset of 30 samples were selected to undergo both ICP-MS analysis as well as XRF analysis in order to determine the statistical accuracy of the XRF data. Although over 5000 samples have been analyzed over the course of this study, these data are proprietary and owned by Acadian Mining. They have permitted the release of this representative data set, as well as the corresponding gold values which were obtained prior to the implementation of this study by fire assay. All values are reported in ppm, unless stated otherwise.

	Representative XRF data						
Sample	**10228**	**10230**	**10252**	**22247**	**8677**	**10785**	**22345**
P	957	-940	-1642	116	-2736	-2382	-1570
P +/-	1159	716	1129	1122	1046	770	1121
S	9035	3368	6664	7470	3135	1469	5582
S +/-	448	274	440	429	328	236	418
Cl	986	525	1642	1273	993	374	1665
Cl +/-	91	70	105	98	90	72	108
K	20364	13316	33951	21681	27563	13297	37743
K +/-	208	146	309	222	250	148	335
Ca	18232	326	4514	13128	16110	6575	4525
Ca +/-	162	37	88	135	149	82	89
Ti	3518	1691	4476	3724	4320	3564	4772
Ti +/-	39	24	48	41	43	36	50
V	60	37	106	82	86	55	108
V +/-	4	2	5	4	4	3	5
Cr	61	44	94	67	76	56	102
Cr +/-	4	3	5	5	4	3	6
Mn	861	229	754	619	688	466	645
Mn +/-	10	5	10	9	9	7	10
Fe	42531	25843	63396	44935	44336	25700	61383
Fe +/-	204	119	300	220	212	119	294
Co	17	11	26	18	17	11	26
Co +/-	1	1	1	1	1	1	1
Ni	-19	-14	-61	-16	-31	-16	-55
Ni +/-	4	3	5	5	4	3	5
Cu	54	24	58	58	28	10	60
Cu +/-	3	2	3	3	2	2	3
Zn	68	39	97	73	78	44	109
Zn +/-	2	2	3	2	2	2	3
As	842	289	15	5280	3407	72	126
As +/-	16	7	3	41	28	3	5
Se	-6	-3	-8	-14	-11	-4	-6
Se +/-	1	1	1	1	1	1	1
Rb	91	59	132	88	105	63	139
Rb +/-	1	1	1	1	1	1	2
Sr	172	40	105	138	133	127	55
Sr +/-	3	1	2	2	2	2	2
Y	34	20	42	32	41	37	37

Sample	10228	10230	10252	22247	8677	10785	22345
Y +/-	2	1	1	1	1	1	1
Zr	160	65	131	219	228	266	136
Zr +/-	2	1	2	3	3	3	2
Nb	16	11	23	17	22	18	20
Nb +/-	1	1	1	1	1	1	1
Mo	2	1	0	0	2	2	1
Mo +/-	1	1	1	1	1	1	1
Rh	0	2	1	0	0	1	1
Rh +/-	1	1	1	1	1	1	1
Pd	3	3	2	1	2	3	1
Pd +/-	1	1	1	1	1	1	1
W							
W +/-							
Cd	1	2	1	0	0	2	2
Cd +/-	2	2	2	2	2	2	2
Sn	3	0	7	0	-1	-7	-1
Sn +/-	4	3	4	4	4	3	4
Sb	-1	-7	-2	6	1	6	0
Sb +/-	4	3	4	4	4	3	4
Ba	275	222	455	355	441	213	483
Ba +/-	13	11	13	13	13	12	14
La	7	-18	16	25	21	7	-2
La +/-	17	16	18	18	17	16	18
Ce	37	54	53	52	51	44	50
Ce +/-	27	25	28	28	27	25	28
Pr	-10	-34	-7	-98	-42	10	-53
Pr +/-	29	26	30	30	29	26	30
Nd	5	30	78	53	30	37	22
Nd +/-	29	26	29	30	29	26	30
Sm	10	43	37	41	15	12	45
Sm +/-	22	20	23	24	22	20	23
Pt	4	3	16	-15	-7	6	13
Pt +/-	2	2	2	3	2	2	2
Au	53	17	3	154	103	2	7
Au +/-	4	2	1	7	6	1	2
Hg	-9	-5	-2	-29	-21	-1	-3
Hg +/-	2	1	2	3	2	1	2
Pb	1664	287	42	21	14	9	36

Sample	10228	10230	10252	22247	8677	10785	22345
Pb +/-	11	3	2	2	1	1	2
Bi	41	15	13	14	18	11	15
Bi +/-	3	1	1	1	1	1	2
U	4	3	2	-2	-2	3	2
U +/-	2	1	2	2	2	1	2

	Representative XRF data						
Sample	11185	22232	22258	22246	11105	11103	11075
P	-1243	-2402	-741	635	-2366	-2104	-764
P +/-	1120	995	677	812	1138	1141	916
S	5273	4191	933	1020	5214	6597	2351
S +/-	413	342	196	212	396	449	287
Cl	1632	742	126	-29	1160	1567	690
Cl +/-	110	85	64	63	99	109	88
K	37635	18306	10380	9812	34795	42109	12353
K +/-	338	193	125	125	308	368	155
Ca	4418	14121	2857	8813	15777	3838	8679
Ca +/-	90	136	54	94	156	88	103
Ti	4923	3181	2551	2424	4525	5432	4081
Ti +/-	52	36	28	28	47	55	42
V	98	73	43	40	104	117	57
V +/-	5	3	3	3	4	5	4
Cr	101	61	37	37	81	107	55
Cr +/-	5	4	3	3	5	6	4
Mn	658	604	211	271	664	592	403
Mn +/-	10	8	5	5	9	10	7
Fe	59495	36553	16862	18130	46527	63084	29032
Fe +/-	298	175	83	91	225	311	151
Co	23	14	6	7	19	23	12
Co +/-	1	1	0	0	1	1	1
Ni	-39	-28	-8	-8	-35	-32	-24
Ni +/-	5	4	3	3	5	5	4
Cu	60	42	6	12	31	55	11
Cu +/-	3	3	2	2	3	3	2
Zn	101	60	27	32	73	106	52
Zn +/-	3	2	2	2	2	3	2
As	6903	1167	1142	3401	1539	3061	10968

Sample	11185	22232	22258	22246	11105	11103	11075
As +/-	54	13	12	26	16	28	80
Se	-17	-8	-5	-7	-11	-15	-14
Se +/-	2	1	1	1	1	1	2
Rb	129	85	47	42	140	160	44
Rb +/-	2	1	1	1	2	2	1
Sr	79	237	73	93	104	83	80
Sr +/-	2	3	2	2	2	2	2
Y	35	35	33	29	37	41	35
Y +/-	2	1	1	1	1	2	1
Zr	147	166	238	241	198	149	279
Zr +/-	2	2	3	3	3	2	3
Nb	25	15	16	14	20	24	20
Nb +/-	1	1	1	1	1	1	1
Mo	3	1	3	1	2	3	3
Mo +/-	1	1	1	1	1	1	1
Rh	1	0	0	1	0	1	1
Rh +/-	1	1	0	1	1	1	1
Pd	2	2	2	2	3	2	2
Pd +/-	1	1	1	1	1	1	1
W							
W +/-							
Cd	2	-2	3	1	1	1	4
Cd +/-	2	2	2	2	2	2	2
Sn	0	3	-4	-7	-8	-4	-5
Sn +/-	4	4	3	3	4	4	4
Sb	10	0	3	6	1	-8	2
Sb +/-	4	4	3	3	4	4	4
Ba	499	368	156	162	466	556	191
Ba +/-	14	13	11	12	14	15	13
La	5	28	24	0	48	35	21
La +/-	19	17	16	16	18	19	18
Ce	-1	38	43	-17	75	79	86
Ce +/-	29	27	25	26	28	29	28
Pr	-22	-44	12	-66	-68	-106	45
Pr +/-	31	29	26	27	29	31	29
Nd	36	42	33	14	66	114	35
Nd +/-	31	28	26	27	29	30	29
Sm	64	57	-18	26	-5	36	41

Sample	11185	22232	22258	22246	11105	11103	11075
Sm +/-	24	22	20	21	22	24	22
Pt	-18	6	2	-10	8	3	-45
Pt +/-	3	2	2	2	2	3	3
Au	188	31	27	80	52	91	270
Au +/-	9	3	3	5	4	6	10
Hg	-38	-4	-5	-19	-11	-20	-58
Hg +/-	3	2	2	2	2	2	4
Pb	20	22	16	15	18	25	30
Pb +/-	2	1	1	1	1	2	2
Bi	20	12	8	10	13	17	20
Bi +/-	2	1	1	1	1	2	1
U	-4	0	4	2	0	-1	-6
U +/-	2	2	1	1	2	2	2

	Representative XRF data						
Sample	11089	11098	21928	11285	11294	11061	11282
P	-2481	-2881	741	5836	183	2854	112
P +/-	1364	1233	1468	1590	1333	1433	1285
S	6549	8013	10022	11326	5867	8020	6050
S +/-	482	501	573	622	475	530	466
Cl	1618	1860	2272	2329	1722	1918	1888
Cl +/-	117	120	135	145	125	135	127
K	45253	37878	40864	53246	58519	45838	47982
K +/-	405	356	393	501	506	433	431
Ca	16927	7655	12861	7514	5383	8689	7566
Ca +/-	179	117	159	132	111	133	121
Ti	5859	5426	6107	6256	6863	7202	5796
Ti +/-	61	58	65	69	69	73	61
V	129	116	135	160	176	147	124
V +/-	5	5	6	6	6	6	5
Cr	112	117	161	140	132	126	120
Cr +/-	6	6	7	7	7	7	6
Mn	958	660	814	603	707	529	597
Mn +/-	13	11	12	11	11	10	10
Fe	71971	70159	82255	85468	75160	70007	64464
Fe +/-	373	367	455	522	414	410	360
Co	28	28	31	31	27	24	25

Sample	11089	11098	21928	11285	11294	11061	11282
Co +/-	1	1	1	1	1	1	1
Ni	-45	-47	-41	-35	-34	-19	-46
Ni +/-	6	6	7	8	7	7	6
Cu	109	80	47	59	38	30	46
Cu +/-	4	4	4	4	3	4	4
Zn	131	107	108	149	149	152	124
Zn +/-	3	3	4	5	4	4	4
As	8803	10594	19398	41292	19963	31221	25361
As +/-	71	84	153	331	156	247	194
Se	-22	-24	-34	-54	-35	-46	-35
Se +/-	2	2	2	3	2	3	2
Rb	141	129	105	126	164	126	158
Rb +/-	2	2	2	2	2	2	2
Sr	156	98	145	62	85	112	86
Sr +/-	3	2	3	2	2	3	2
Y	47	46	52	43	50	57	45
Y +/-	2	2	2	2	2	2	2
Zr	179	162	235	158	170	244	145
Zr +/-	3	3	3	3	3	3	2
Nb	25	23	25	25	27	27	21
Nb +/-	2	2	2	2	2	2	2
Mo	0	3	5	6	5	7	5
Mo +/-	1	1	1	1	1	1	1
Rh	2	0	-1	0	0	1	0
Rh +/-	1	1	1	1	1	1	1
Pd	4	1	1	3	2	2	2
Pd +/-	1	1	1	1	1	1	1
W							
W +/-							
Cd	4	3	3	-2	-3	3	-1
Cd +/-	2	2	2	2	2	2	2
Sn	-2	0	2	5	16	4	2
Sn +/-	4	4	4	4	4	4	4
Sb	-3	8	-2	14	5	10	9
Sb +/-	4	4	4	4	4	4	4
Ba	600	475	558	607	744	565	547
Ba +/-	16	15	16	17	17	16	16
La	47	22	4	12	32	10	14

Sample	11089	11098	21928	11285	11294	11061	11282
La +/-	20	19	21	22	21	21	20
Ce	0	92	86	54	77	82	-28
Ce +/-	31	30	33	35	32	32	32
Pr	-140	-22	-98	-71	-114	-35	-67
Pr +/-	33	32	36	37	35	34	34
Nd	58	26	19	114	117	28	105
Nd +/-	32	32	35	36	34	34	33
Sm	26	46	16	14	-7	68	25
Sm +/-	25	25	28	29	27	27	27
Pt	-23	-36	-76	-113	-60	-89	-79
Pt +/-	3	3	4	6	4	6	5
Au	224	295	512	752	442	628	537
Au +/-	10	11	16	26	16	21	18
Hg	-49	-64	-120	-194	-92	-143	-105
Hg +/-	4	4	5	9	6	7	6
Pb	22	23	53	50	48	91	46
Pb +/-	2	2	2	3	2	3	2
Bi	24	25	33	41	25	38	29
Bi +/-	2	2	2	2	2	2	2
U	-5	-7	-12	-16	-7	-15	-17
U +/-	2	2	2	2	2	2	2

	Representative XRF data						
Sample	22228	13459	11018	11257	22075	22249	11305
P	-1041	-812	-1057	-1767	83	-586	-843
P +/-	1199	1166	1256	1122	930	852	900
S	3466	4392	10639	790	6040	2645	1166
S +/-	383	398	532	286	354	278	229
Cl	1567	1621	2041	1153	495	464	194
Cl +/-	111	107	117	96	78	77	69
K	49245	37668	32875	27823	17679	12014	11632
K +/-	412	337	310	260	180	146	136
Ca	9212	6136	9013	17421	11190	7078	18894
Ca +/-	124	101	120	162	113	88	150
Ti	5546	4637	4857	4349	3435	2939	3180
Ti +/-	56	50	52	45	36	33	32
V	117	116	116	107	66	53	52

Sample	22228	13459	11018	11257	22075	22249	11305
V +/-	5	5	5	4	3	3	3
Cr	110	105	90	81	70	55	45
Cr +/-	6	6	6	5	4	4	3
Mn	617	747	838	896	418	355	576
Mn +/-	10	11	11	11	7	6	7
Fe	57897	63744	71169	45603	27210	26409	18655
Fe +/-	282	310	351	217	131	133	92
Co	22	25	29	18	11	9	7
Co +/-	1	1	1	1	1	1	0
Ni	-45	-59	-63	-8	-16	-3	-4
Ni +/-	5	5	6	5	4	4	3
Cu	30	36	111	36	31	19	11
Cu +/-	3	3	4	3	2	2	2
Zn	106	107	87	82	55	41	35
Zn +/-	3	3	3	2	2	2	2
As	1073	235	4179	10	838	8337	551
As +/-	13	6	34	3	10	58	8
Se	-11	-8	-14	-8	-8	-9	-4
Se +/-	1	1	1	1	1	1	1
Rb	172	148	119	124	71	47	57
Rb +/-	2	2	1	1	1	1	1
Sr	119	87	97	228	107	115	117
Sr +/-	2	2	2	3	2	2	2
Y	40	39	46	45	38	30	34
Y +/-	2	2	2	1	1	1	1
Zr	159	148	148	157	188	288	247
Zr +/-	2	2	2	2	2	3	3
Nb	25	25	20	23	17	13	17
Nb +/-	1	1	1	1	1	1	1
Mo	1	3	0	2	1	1	1
Mo +/-	1	1	1	1	1	1	1
Rh	1	1	0	0	1	1	1
Rh +/-	1	1	1	1	1	1	1
Pd	1	5	0	2	0	-1	2
Pd +/-	1	1	1	1	1	1	1
W							
W +/-							
Cd	6	4	1	1	1	0	0

Sample	22228	13459	11018	11257	22075	22249	11305
Cd +/-	2	2	2	2	2	2	2
Sn	0	-4	3	0	-9	6	-2
Sn +/-	4	4	4	4	3	3	3
Sb	5	-2	0	-6	0	6	11
Sb +/-	4	4	4	4	4	4	3
Ba	683	556	526	539	305	177	197
Ba +/-	15	15	14	14	12	12	12
La	8	26	59	11	32	-1	13
La +/-	18	19	19	18	17	17	16
Ce	2	80	82	42	50	42	60
Ce +/-	29	29	29	28	26	27	25
Pr	-90	-64	-50	-79	-72	-57	-18
Pr +/-	31	31	31	30	28	29	27
Nd	125	76	77	54	56	3	22
Nd +/-	30	30	31	29	27	28	27
Sm	50	7	-19	22	40	35	-5
Sm +/-	24	23	25	23	21	22	21
Pt	11	15	-6	14	8	-24	0
Pt +/-	2	2	3	2	2	3	2
Au	38	5	123	2	26	168	21
Au +/-	4	2	7	1	3	9	2
Hg	-4	2	-24	-5	-1	-36	-8
Hg +/-	2	2	3	1	2	3	1
Pb	16	14	36	16	32	20	11
Pb +/-	2	2	2	1	1	1	1
Bi	17	14	21	11	10	13	12
Bi +/-	2	2	2	1	1	1	1
U	-1	1	-2	1	3	-3	3
U +/-	2	2	2	2	1	1	1

	Representative XRF data		
Sample	25909	25906	22301
P	-1515	-1507	-565
P +/-	653	666	525
S	1107	914	196
S +/-	192	195	132
Cl	24	116	-317

Sample	25909	25906	22301
Cl +/-	61	61	43
K	5804	3773	263
K +/-	90	74	30
Ca	6382	3647	2000
Ca +/-	74	57	39
Ti	2636	2245	127
Ti +/-	28	26	7
V	26	21	1
V +/-	2	2	1
Cr	41	31	4
Cr +/-	3	3	2
Mn	244	332	91
Mn +/-	5	5	3
Fe	12698	19499	7312
Fe +/-	64	93	41
Co	6	8	3
Co +/-	0	0	0
Ni	-8	-16	-9
Ni +/-	3	3	2
Cu	4	10	-2
Cu +/-	2	2	2
Zn	66	38	-7
Zn +/-	2	2	1
As	0	28	145
As +/-	5	3	4
Se	-1	-1	0
Se +/-	1	1	1
Rb	33	20	2
Rb +/-	1	1	0
Sr	85	68	6
Sr +/-	2	2	1
Y	33	25	7
Y +/-	1	1	1
Zr	96	384	25
Zr +/-	2	3	1
Nb	16	15	5
Nb +/-	1	1	1
Mo	3	3	0

Sample	25909	25906	22301
Mo +/-	1	1	1
Rh	1	1	1
Rh +/-	1	1	0
Pd	4	3	3
Pd +/-	1	1	1
W			
W +/-			
Cd	1	3	0
Cd +/-	2	2	2
Sn	-14	-14	-5
Sn +/-	3	3	3
Sb	-4	-3	-3
Sb +/-	3	3	3
Ba	116	57	28
Ba +/-	11	11	10
La	15	-1	-9
La +/-	15	15	15
Ce	34	65	6
Ce +/-	24	24	23
Pr	11	22	36
Pr +/-	25	25	24
Nd	40	44	18
Nd +/-	24	25	24
Sm	36	22	2
Sm +/-	19	19	19
Pt	-1	0	-3
Pt +/-	1	1	1
Au	2	3	7
Au +/-	1	1	1
Hg	-6	-6	-5
Hg +/-	1	1	1
Pb	227	30	-1
Pb +/-	3	1	1
Bi	16	12	1
Bi +/-	1	1	1
U	4	6	1
U +/-	1	1	1

Representative ICP-MS data				
SAMPLE	**BD06-110-10228**	**BD06-110-10230**	**BD06-110-10252**	**BD09-152-8677**
Ag	22.2	4.14	0.55	0.17
Al (%)	6.06	3.44	8.41	7.47
As	1070	372	25.6	3950
Ba	310	240	510	480
Be	1.38	0.84	2.18	2.21
Bi	33	6.38	0.57	0.36
Ca (%)	1.8	0.1	0.5	1.53
Cd	0.92	0.33	0.12	0.13
Ce	58.4	29.4	63.4	64.6
Co	18.9	11.4	21.4	14.1
Cr	50	38	72	60
Cs	8.48	2.65	5.35	7.85
Cu	56.9	34.3	72.1	30.8
Fe (%)	4.34	3.05	6.13	4.26
Ga	15.95	10.2	25.5	22
Ge	0.14	0.11	0.19	0.18
Hf	2.7	1.5	3.6	3.9
In	0.049	0.035	0.077	0.063
K (%)	1.72	1.26	2.83	2.45
La	30.9	16	33.2	32.5
Li	26.1	14.4	37.2	59.7
Mg (%)	0.86	0.52	1.31	1.19
Mn	925	273	754	675
Mo	0.33	0.62	0.42	0.18
Na (%)	0.86	0.27	0.49	1.36
Nb	10.4	5.7	12.9	12.1
Ni	33.2	18.4	40	26.1
P	280	170	450	290
Pb	1795	299	44.6	11.5
Rb	88.9	58.5	120	93.9
Re	<0.002	<0.002	<0.002	<0.002
S (%)	1.13	0.55	0.78	0.57
Sb	0.8	0.45	0.15	2.46
Sc	11.5	7	19.7	14.9
Se	1	<1	1	1
Sn	2.2	2.1	2.7	2.2
Sr	162.5	37.9	100.5	129.5

SAMPLE	BD06-110-10228	BD06-110-10230	BD06-110-10252	BD09-152-8677
Ta	0.69	0.36	0.91	0.85
Te	0.81	0.61	0.09	0.14
Th	8.2	5	11	10.3
Ti (%)	0.359	0.189	0.453	0.43
Tl	0.79	0.34	0.7	0.53
U	1.5	0.9	1.9	1.8
V	64	42	108	80
W	5.9	5.2	7.5	5.4
Y	18	7.3	24.6	19.4
Zn	59	44	100	76
Zr	90.3	58.9	113.5	124

Representative ICP-MS data				
SAMPLE	BD09-146-10785	BD07-138-22345	BD06-115-11185	BD07-137-22232
Ag	0.09	0.72	0.8	0.19
Al (%)	5.72	8.95	8.52	6.33
As	76.9	183.5	8130	1575
Ba	280	580	570	420
Be	1.03	2.14	2.63	1.64
Bi	0.12	3.21	0.95	0.25
Ca (%)	0.8	0.47	0.47	1.55
Cd	0.05	0.14	0.08	0.1
Ce	55.9	80.3	76.7	57.5
Co	9.6	27.2	25.8	17.9
Cr	51	83	79	55
Cs	5.22	10.8	8.64	6.36
Cu	15.5	89	62.8	52.9
Fe (%)	2.87	6.12	5.58	4.02
Ga	15.05	26.6	26	17.85
Ge	0.15	0.22	0.21	0.15
Hf	3.5	3.5	3.6	2.7
In	0.044	0.084	0.08	0.079
K (%)	1.33	3.15	3.11	1.65
La	29.1	41.2	39.6	30.3
Li	24.2	69.7	62.6	33.3
Mg (%)	0.74	1.59	1.49	0.93

SAMPLE	BD09-146-10785	BD07-138-22345	BD06-115-11185	BD07-137-22232
Mn	533	602	611	704
Mo	0.35	0.48	0.3	0.5
Na (%)	1.92	0.4	0.73	1.36
Nb	10.2	13.7	13	10.1
Ni	16.1	52	40.5	24.5
P	220	460	380	260
Pb	11	45	16.2	20.8
Rb	65.5	135.5	124.5	90
Re	<0.002	<0.002	<0.002	<0.002
S (%)	0.14	0.89	1.02	0.61
Sb	0.13	0.23	4.67	1.9
Sc	11.3	22.4	19.2	13.9
Se	<1	1	1	<1
Sn	1.6	3	2.5	1.6
Sr	118	52.8	73.6	234
Ta	0.75	0.87	0.88	0.63
Te	<0.05	0.88	0.66	0.5
Th	8.8	10.4	11.5	8.1
Ti (%)	0.414	0.47	0.459	0.345
Tl	0.33	0.65	0.64	0.51
U	2	1.9	1.8	1.7
V	61	115	98	74
W	3	7.4	7.5	3.2
Y	11.9	24.9	14.5	16.8
Zn	46	123	101	65
Zr	109.5	116	117	92.8

Representative ICP-MS data				
SAMPLE	BD07-137-22258	BD07-137-22246	BD06-114-11105	BD06-114-11103
Ag	0.07	0.1	0.1	0.17
Al (%)	4.28	4.34	7.97	9.09
As	1440	4100	1755	3480
Ba	210	190	510	650
Be	0.93	0.89	2.09	2.57
Bi	0.16	0.18	0.44	0.67

SAMPLE	BD07-137-22258	BD07-137-22246	BD06-114-11105	BD06-114-11103
Ca (%)	0.4	1	1.47	0.38
Cd	0.05	0.09	0.08	0.1
Ce	48.1	48.7	70.7	63.2
Co	6.9	7.8	20.6	26
Cr	39	39	63	78
Cs	2.31	2.95	8.24	5.73
Cu	11.7	10.2	40.1	67.6
Fe (%)	2.03	2.13	4.56	5.82
Ga	10.7	10.15	22.1	27.2
Ge	0.14	0.11	0.17	0.22
Hf	2.8	2.7	3.4	3.6
In	0.031	0.034	0.064	0.081
K (%)	1.05	1	2.97	3.57
La	25.5	25.3	37.9	29.9
Li	17.6	14.6	71.1	80.2
Mg (%)	0.49	0.45	1.22	1.52
Mn	249	311	636	521
Mo	0.61	0.43	0.53	1.17
Na (%)	1.25	1.5	0.76	0.56
Nb	7.4	6.2	12.5	14.7
Ni	11.9	10.1	31	44.7
P	170	180	330	440
Pb	15.9	16.1	17.4	20.9
Rb	53.5	49.1	135	138.5
Re	<0.002	<0.002	<0.002	<0.002
S (%)	0.14	0.25	0.76	0.86
Sb	1.38	4.09	1.29	2.31
Sc	7.8	7.6	17.2	21.4
Se	<1	<1	<1	1
Sn	1.2	1.1	2.3	2.6
Sr	71.1	93.6	100.5	78.9
Ta	0.5	0.44	0.8	0.95
Te	0.1	0.63	0.11	0.3
Th	7.8	6.7	10.1	9.3
Ti (%)	0.291	0.281	0.423	0.512
Tl	0.25	0.23	0.7	0.81
U	1.9	1.7	1.8	2
V	42	42	91	113

SAMPLE	BD07-137-22258	BD07-137-22246	BD06-114-11105	BD06-114-11103
W	2.3	3.5	5.8	5.6
Y	8.8	13.1	15.7	20.1
Zn	33	36	78	108
Zr	92.1	87.1	113	115

Representative ICP-MS data				
SAMPLE	BD06-114-11075	BD06-114-11089	BD06-114-11098	BD07-136-21928
Ag	0.28	0.29	0.09	0.64
Al (%)	4.9	9.52	8.68	9.32
As	10000	9540	10000	10000
Ba	210	660	560	560
Be	0.87	2.43	3	2.44
Bi	0.94	1.21	0.74	4.67
Ca (%)	0.87	1.49	0.7	1.12
Cd	0.12	0.34	0.1	0.12
Ce	52.2	65.7	90.9	91.9
Co	7.3	30.3	28.6	40
Cr	42	85	74	86
Cs	3.92	12.9	8.16	6.91
Cu	4.3	120	69.8	19.5
Fe (%)	2.91	6.09	6.1	7
Ga	11.85	28.1	25.3	26.7
Ge	0.14	0.21	0.22	0.24
Hf	3.2	3.9	3.6	4.4
In	0.046	0.088	0.085	0.113
K (%)	1.11	3.6	3	2.73
La	27	32.7	46.8	47.2
Li	29.5	94.5	71.6	51
Mg (%)	0.62	1.68	1.49	1.32
Mn	377	853	600	727
Mo	1.6	0.15	0.33	1.52
Na (%)	1.58	1.18	0.84	1.59
Nb	6.6	15.5	14.7	17.9
Ni	13.4	49.2	53.1	68.3
P	210	430	390	570

SAMPLE	BD06-114-11075	BD06-114-11089	BD06-114-11098	BD07-136-21928
Pb	24.9	16.5	15.2	42.6
Rb	53	144.5	129	118
Re	<0.002	<0.002	<0.002	<0.002
S (%)	0.54	1.14	1.33	1.73
Sb	3.96	2.25	7.12	4.99
Sc	8.9	23.1	20.2	22.1
Se	<1	1	2	2
Sn	1.7	3	2.6	3
Sr	73.9	150.5	97.5	139.5
Ta	0.47	0.98	0.93	1.13
Te	1.16	0.5	1.1	4.69
Th	7.5	12.4	11.1	11.3
Ti (%)	0.348	0.531	0.481	0.533
Tl	0.25	0.78	0.66	0.56
U	1.7	2	2	2.4
V	44	105	100	117
W	5.9	8	5.2	7.4
Y	10.2	26.3	22	17.2
Zn	40	122	99	92
Zr	103.5	132.5	122	143

Representative ICP-MS data				
SAMPLE	BD06-116-11285	BD06-116-11294	BD06-114-11061	BD06-116-11282
Ag	1.05	0.25	0.21	0.39
Al (%)	8.69	10.2	9.55	8.65
As	10000	10000	10000	10000
Ba	650	800	620	580
Be	2.16	2.72	2.42	2.32
Bi	5.84	1.45	2.53	1.96
Ca (%)	0.55	0.44	0.68	0.62
Cd	0.08	0.08	0.31	0.12
Ce	99.8	69.6	85.3	78.1
Co	29.8	27.7	21.4	25.4
Cr	85	102	86	81
Cs	9.99	9.25	13.2	18.15
Cu	22.2	24.6	2.9	26.4

SAMPLE	BD06-116-11285	BD06-116-11294	BD06-114-11061	BD06-116-11282
Fe (%)	6.2	5.9	5.33	5.05
Ga	28.6	34.2	29.5	27.1
Ge	0.26	0.24	0.23	0.2
Hf	3.7	4	4.5	3.5
In	0.127	0.124	0.121	0.111
K (%)	3.46	4.21	3.32	3.42
La	52.8	33.4	44.1	41
Li	56.2	62.8	60.3	63.7
Mg (%)	1.4	1.65	1.49	1.44
Mn	431	581	415	444
Mo	0.61	1.61	1.14	0.59
Na (%)	0.74	0.8	1.79	0.97
Nb	13.1	16.4	15.8	13.4
Ni	51.9	53.1	35.4	32.9
P	320	430	290	320
Pb	32	35.4	78	33.6
Rb	142	145	143	164.5
Re	<0.002	<0.002	<0.002	<0.002
S (%)	1.84	1.15	1.37	1.18
Sb	17.25	6.86	10.9	11.45
Sc	19.6	24.4	21.7	19.4
Se	2	1	1	2
Sn	3.5	4.2	3.6	3.1
Sr	60.6	74.5	105	81.9
Ta	0.84	1.01	1.01	0.9
Te	5.23	2.54	3.96	2.53
Th	11.6	10.2	12.1	10.9
Ti (%)	0.446	0.575	0.567	0.446
Tl	0.58	0.73	0.65	0.94
U	1.9	2.1	2.5	1.6
V	104	136	117	100
W	9.4	10.7	12.2	8.8
Y	15.3	20.1	13.5	14.8
Zn	80	121	104	91
Zr	122.5	135.5	150.5	119

Representative ICP-MS data				
SAMPLE	**BD07-137-22228**	**BD07-136-13459**	**BD06-113-11018**	**BD06-116-11257**
Ag	0.11	0.08	0.48	0.1
Al (%)	9.27	9.06	8.07	8.17
As	1350	240	5110	11.6
Ba	710	650	560	550
Be	2.84	2.54	2.2	2.2
Bi	0.15	0.28	1.57	0.19
Ca (%)	0.92	0.64	0.88	1.64
Cd	0.08	0.06	0.18	0.06
Ce	66	72.7	98.8	59.2
Co	19	21.2	25.5	20
Cr	80	79	65	66
Cs	10.85	5.39	6.22	5.67
Cu	38.5	48.3	120	46.1
Fe (%)	5.53	6.04	6.56	4.39
Ga	28.2	26.3	21.8	23.2
Ge	0.22	0.22	0.24	0.18
Hf	3.8	3.3	3.3	2.2
In	0.084	0.077	0.067	0.064
K (%)	4.01	3.23	2.67	2.46
La	32.1	36.6	57.4	29.6
Li	52.4	46.2	48.5	44.8
Mg (%)	1.57	1.49	1.34	1.45
Mn	616	787	783	906
Mo	0.14	0.25	0.5	0.23
Na (%)	0.85	0.47	0.99	1.89
Nb	15.6	14.4	12.6	12.7
Ni	35	37.4	46.5	40.4
P	410	390	400	730
Pb	12.9	14.3	38.3	13.2
Rb	143.5	132.5	123.5	91.2
Re	<0.002	<0.002	<0.002	<0.002
S (%)	0.45	0.61	1.5	0.13
Sb	1.02	0.3	5.02	0.12
Sc	22.7	20.1	18.7	17.9
Se	1	1	1	1
Sn	2.9	2.6	2.3	2.2
Sr	111.5	80	104	210

SAMPLE	BD07-137-22228	BD07-136-13459	BD06-113-11018	BD06-116-11257
Ta	0.97	0.93	0.82	0.84
Te	<0.05	0.07	0.5	0.05
Th	10.6	11.1	9.5	8.9
Ti (%)	0.527	0.493	0.447	0.443
Tl	0.84	0.7	0.96	0.6
U	2.1	1.9	1.9	1.8
V	111	104	94	97
W	6.6	7.2	7.9	1.6
Y	20.5	23.5	25.5	20.3
Zn	112	113	85	88
Zr	130	117.5	111.5	74.8

Representative ICP-MS data				
SAMPLE	BD07-137-22075	BD07-137-22249	BD06-116-11305	BD09-146-25909
Ag	0.33	0.11	0.13	4.67
Al (%)	5.84	4.44	4.88	2.86
As	1000	9640	615	10.2
Ba	330	210	220	120
Be	1.33	0.93	0.89	0.66
Bi	0.58	0.21	0.19	12.2
Ca (%)	1.06	0.78	1.86	0.73
Cd	0.23	0.09	0.09	0.2
Ce	59.8	46.3	62.3	25.7
Co	12.9	12.3	8	2.8
Cr	63	41	44	52
Cs	6.57	3.46	3.33	2.38
Cu	36.6	12.8	11.8	8.6
Fe (%)	2.97	2.83	2.07	1.47
Ga	16.65	11.1	11.6	7.14
Ge	0.16	0.15	0.15	0.1
Hf	2.6	3.1	3	1.7
In	0.048	0.043	0.034	0.015
K (%)	1.52	1.1	1.12	0.59
La	30.6	24.1	32.1	12.8
Li	38.3	18.1	30.7	15.6
Mg (%)	0.75	0.51	0.54	0.26
Mn	464	392	595	301

SAMPLE	BD07-137-22075	BD07-137-22249	BD06-116-11305	BD09-146-25909
Mo	1.6	0.7	0.29	2.57
Na (%)	1.65	1.38	1.56	0.93
Nb	9.3	7.8	8.2	7.2
Ni	17.3	14.8	14	5.1
P	310	170	370	50
Pb	32.5	14.8	13.3	234
Rb	74	58	59.2	35.5
Re	<0.002	<0.002	<0.002	<0.002
S (%)	0.89	0.53	0.14	0.08
Sb	0.29	9.75	0.42	0.12
Sc	11.3	8.8	8.8	8.8
Se	1	1	<1	<1
Sn	2.4	1.2	1.3	1.5
Sr	102	116	110	79.8
Ta	0.61	0.5	0.56	0.55
Te	0.19	2.14	<0.05	2.12
Th	7.8	7.4	8.8	5.1
Ti (%)	0.35	0.317	0.351	0.315
Tl	0.36	0.26	0.27	0.18
U	1.8	1.8	2	3.2
V	64	43	51	38
W	12.9	2.6	2.8	4.2
Y	11.6	12.4	14.1	8.2
Zn	55	37	40	20
Zr	87.2	104	96.4	59.5

Representative ICP-MS data		
SAMPLE	BD09-146-25906	BD07-138-22301
Ag	0.23	0.03
Al (%)	2.38	0.22
As	30.2	184
Ba	70	10
Be	0.42	0.06
Bi	0.37	0.02
Ca (%)	0.48	0.3
Cd	0.07	0.04

SAMPLE	BD09-146-25906	BD07-138-22301
Ce	37.5	3.45
Co	4.8	6.3
Cr	31	16
Cs	1.69	0.15
Cu	12.6	6.5
Fe (%)	2.31	1.03
Ga	5.62	0.96
Ge	0.11	<0.05
Hf	3.3	0.3
In	0.01	<0.005
K (%)	0.37	0.04
La	18.9	1.7
Li	19.1	4.6
Mg (%)	0.31	0.07
Mn	404	121
Mo	0.87	0.4
Na (%)	0.89	0.06
Nb	5.2	0.6
Ni	6.3	2.1
P	80	10
Pb	29.6	1.9
Rb	22	2
Re	<0.002	<0.002
S (%)	0.08	0.04
Sb	0.13	0.14
Sc	4.9	0.4
Se	<1	1
Sn	0.7	0.2
Sr	65.9	7.1
Ta	0.35	<0.05
Te	0.1	<0.05
Th	7.5	0.4
Ti (%)	0.265	0.015
Tl	0.12	0.02
U	1.8	0.1
V	23	2
W	0.9	0.3
Y	8.1	1.3

SAMPLE	BD09-146-25906	BD07-138-22301
Zn	24	6
Zr	107	9.3

Representative fire assay data								
Hole ID	BD06-110	BD06-110	BD06-110	BD07-137	BD09-152	BD09-146	BD07-138	BD06-115
length	1	1	1	1	1	1	1	1
Sample	10228	10230	10252	22247	8677	10785	22345	11185
Au Coarse	22000	713	275	37.3	0.01	0.01	23.3	403
Au Fine	63.7	10.8	0.5	0.71	0.01	0.01	1.49	4.32
Au Coarse (mg)	42.188	1.643	0.862	0.265	0.001	0.001	0.83	16.596
Wt Coarse (mg)	1.92	2.3	3.13	7.1	39.72	30.77	35.59	41.17
Wt fine (g)	1748	1858.5	2934	2007	2302	2442	1792.5	2281
Au Fine aa25	58.2	10.1	0.56	0.73	0.01	0.01	1.59	4.44
Au Fine aa25d	69.1	11.45	0.44	0.68	0.01	0.01	1.38	4.19

Representative fire assay data								
Hole ID	BD07-137	BD07-137	BD07-137	BD06-114	BD06-114	BD06-114	BD06-114	BD07-136
length	1	1	1	1	1	1	1	1
Sample	22232	22258	22246	11105	11103	11075	11089	21928
Au Coarse	20.5	9.35	0.77	0.28	0.4	0.74	0.01	0.01
Au Fine	0.38	0.25	0.15	0.08	0.06	0.05	0.01	0.08
Au Coarse (mg)	0.322	0.223	0.023	0.007	0.014	0.011	0.001	0.001
Wt Coarse (mg)	15.71	23.84	30	25.39	34.82	14.87	20.47	47.08
Wt fine (g)	2680	2246	2248	2481	2143	2621	2878	2412
Au Fine aa25	0.3	0.27	0.16	0.08	0.07	0.06	0.01	0.1
Au Fine aa25d	0.45	0.22	0.14	0.08	0.04	0.04	0.01	0.05

Representative fire assay data								
Hole ID	BD06-116	BD06-116	BD06-114	BD06-116	BD07-137	BD07-136	BD06-113	BD06-116
length	1	1	1	1	1	1	1	1
Sample	11285	11294	11061	11282	22228	13459	11018	11257
Au Coarse	593	0.01	0.01	0.01	3.55	5.12	48	0.01
Au Fine	1.21	0.01	0.01	0.01	0.1	0.78	1.65	0.01
Au Coarse (mg)	1.831	0.001	0.001	0.001	0.073	0.14	0.998	0.001
Wt Coarse (mg)	3.09	3.27	16.65	13.18	20.55	27.36	20.77	21.76
Wt fine (g)	1659.5	2044	2450	2244	1773.5	2218	2754	2165
Au Fine aa25	1.15	0.02	0.02	0.03	0.1	0.74	1.41	0.01
Au Fine aa25d	1.27	0.02	0.02	0.01	0.09	0.82	1.88	0.01

Representative fire assay data						
Hole ID	BD07-137	BD07-137	BD06-116	BD09-146	BD09-146	BD07-138
length	1	1	1	1.1	0.1	1
Sample	22075	22249	11305	25909	25906	22301
Au Coarse	0.01	0.01	4.3	0.01	0.01	0.01
Au Fine	0.01	0.01	0.01	0.01	0.01	0.01
Au Coarse (mg)	0.001	0.001	0.128	0.001	0.001	0.001
Wt Coarse (mg)	29.53	1.57	29.78	23.62	3.46	2.46
Wt fine (g)	2496	2367	2008	2984	463.6	2019
Au Fine aa25	0.01	0.01	0.02	0.01	0.01	0.01
Au Fine aa25d	0.02	0.01	0.02	0.01	0.02	0.01

Appendix B:
Cross Sections

Sets of 13 cross sections have been generated to represent the main area of mineralization (800E-1100E). These cross sections contain drill holes that have been systematically logged, sampled at 1 m intervals, and analyzed for Au by fire assay and whole- rock lithogeochemistry. Histograms on the cross sections represent concentrations of elements of interest. These sections are digitally available on the USB drive provided.

Appendix C:
Analysis of the XRF calibration puck

The table below represents 5 analyses of the calibration puck that was provided by INNOV-X Systems to calibrate the energy dispersive XRF spectrometer. These concentrations represent the internal concentrations that the XRF spectrometer uses to determine a sample's margin of error and detection limits. All values are reported in ppm.

Sample	#1	#2	#3	#4	#5
P	58828	56924	79270	49134	63196
P +/-	6210	6227	6726	6053	6379
S	23343	25259	22359	24358	26581
S +/-	1499	1541	1513	1520	1570
Cl	<LOD	<LOD	<LOD	<LOD	<LOD
Cl +/-	1006	978	1008	985	1035
K	<LOD	<LOD	<LOD	<LOD	<LOD
K +/-	396	394	399	386	385
Ca	<LOD	<LOD	<LOD	<LOD	<LOD
Ca +/-	398	400	410	407	406
Ti	<LOD	<LOD	<LOD	<LOD	<LOD
Ti +/-	190	193	197	195	195
V	353	332	362	364	329
V +/-	14	14	14	14	14
Cr	113346	113929	116808	113902	114871
Cr +/-	1217	1229	1273	1225	1241
Mn	7485	7598	7948	7544	7627
Mn +/-	112	114	119	113	114
Fe	1632701	1608143	1626428	1605204	1632863
Fe +/-	19444	18986	19335	18949	19451
Co	375	349	355	367	334
Co +/-	14	13	14	13	14
Ni	96772	96212	96944	96103	97263
Ni +/-	1186	1169	1186	1167	1192
Cu	3467	3436	3414	3300	3445
Cu +/-	85	84	85	83	85

Sample	#1	#2	#3	#4	#5
Zn	86	45	48	54	71
Zn +/-	15	14	14	14	15
As	<LOD	<LOD	<LOD	<LOD	<LOD
As +/-	34	34	34	33	34
Se	20	<LOD	17	<LOD	<LOD
Se +/-	5	15	5	16	16
Rb	38	44	41	41	41
Rb +/-	5	5	5	5	5
Sr	57	57	57	66	66
Sr +/-	4	4	4	4	4
Zr	<LOD	<LOD	12	<LOD	12
Zr +/-	10	10	3	10	4
Mo	20513	20302	20493	21228	20968
Mo +/-	232	228	232	243	240
Ag	<LOD	<LOD	<LOD	<LOD	<LOD
Ag +/-	8	8	8	9	8
Cd	<LOD	<LOD	<LOD	<LOD	<LOD
Cd +/-	9	9	9	9	9
Sn	114	97	107	108	97
Sn +/-	6	6	6	6	6
Sb	<LOD	22	23	<LOD	<LOD
Sb +/-	15	5	5	15	16
Ba	<LOD	<LOD	<LOD	<LOD	<LOD
Ba +/-	74	73	74	76	77
W	224	300	189	251	169
W +/-	56	54	54	54	56
Au	883	808	873	843	984
Au +/-	53	50	52	51	54
Hg	88	61	70	76	65
Hg +/-	16	15	15	15	15
Pb	676	663	682	654	698
Pb +/-	22	22	22	22	22
Bi	654	621	595	611	642
Bi +/-	24	23	23	23	24
Th	<LOD	<LOD	<LOD	<LOD	<LOD
Th +/-	293	290	298	309	296
U	47	69	73	81	61
U +/-	12	12	13	13	12

References

Bierlein, F., Fuller, T., Stuwe, K., Arne, D., & Keays, R. (1998). Wallrock alteration associated with turbidite-hosted gold deposits. Examples from the Palaeozoic Lachlan Fold Belt in central Victoria, Australia. *Ore Geology Reviews* , Vol. 13, 345-380.

Dominy, S. C., Stephenson, P. R., & Annels, A. E. (2002). Classification and Reporting of Mineral Resources for High-Nugget Effect Gold Vein Deposits. *Exploration Mining Geology, Vol. 10* , 215-233.

Dominy, S. (2001). Prediction of gold grade potential in erratic vein-hosted deposits using a geochemical descrimination index. *the Institution of mining and metallurgy* , 110.

Evans, J. (1996). *Straight forward statistics for the behavioral sciences.* Pacific Grove, CA: Brooks/Cole Publishing.

Horne, R. J., & Culshaw, N. (2001). Flexural-slip folding in the Meguma Group, Nova Scotia, Canada. *Journal of Structual Geology* , Vol. 23, 1631-1652.

Horne, R. J., & Pelley, D. (2006). *Geological transect of the Meguma Terrane from Centre Musquodoboit to Tangier* . Nova Scotia : Nova Scotia Department of Natural Resources . Report ME 2007-1, p.71-89

Kontak, D. J., & Smith, P. K. (1993). A metaturbidite-hosted lode gold deposit: The Beaver Dam deposit, Nova Scotia. I. Vein paragenesis and mineral chemistry. *Canadian Mineralogist* , 471-522.

Kontak, D. J., Smith, P. K., Kerrich, R., & Williams, P. F. (1990). Integrated model for Meguma Group lode gold deposits, Nova Scotia, Canada. *Geology* , Vol. 18, 238-242.

Lundell, G., Hillebrand, W. F., Bright, H. A., & Hoffman, J. I. (1962). *Applied inorganic analysis.* New York: John Wiley & Sons, Inc.

McMillan, R. (1996). Turbidite-hosted Au Veins. *Selected British Columbia Mineral Deposit Profiles, Volume II* , 59-62.

Prendergast, K. (2007). Application of lithogeochemistry to gold exploration in the St Ives goldfield, Western Australia. *Geochemistry: Exploration, Environment, Analysis* , Vol. 7, 99-108.

Ramsay, J. G. (1980). The crack-seal mechanism of rock deformation. *Nature* , 135-139.

Rankama, K., & Sahama, T. G. (1950). *Geochemistry.* London: The University of Chicago Press.

Robert, F., Brommecker, R., Bourne, B., Dobak, P., McEwan, C., Rowe, R., et al. (2007). Models and Exploration Methods for Major Gold Deposit Types. *Plenary Session: Ore deposits and exploration technology* , 691-711.

Rollinson, H. (1993). *Using geochemical data: evaluation, presentation, interpretation.* England: Pearson Education Limited.